

# A Novel Multirate Dual-Porosity Model for Improved Simulation of Fractured and Multiporosity Reservoirs

S. Geiger, Heriot-Watt University; M. Dentz, Spanish National Research Council (IDAEA-CSIC); and I. Neuweiler, University of Hannover

## Summary

A major part of the world's remaining oil reserves is in fractured carbonate reservoirs, which are dual-porosity (fracture-matrix) or multiporosity (fracture/vug/matrix) in nature. Fractured reservoirs suffer from poor recovery, high water cut, and generally low performance. They are modeled commonly by use of a dual-porosity approach, which assumes that the high-permeability fractures are mobile and low-permeability matrix is immobile. A single transfer function models the rate at which hydrocarbons migrate from the matrix into the fractures. As shown in many numerical, laboratory, and field experiments, a wide range of transfer rates occurs between the immobile matrix and mobile fractures. These arise, for example, from the different sizes of matrix blocks (yielding a distribution of shape factors), different porosity types, or the inhomogeneous distribution of saturations in the matrix blocks. Thus, accurate models are needed that capture all the transfer rates between immobile matrix and mobile fracture domains, particularly to predict late-time recovery more reliably when the water cut is already high. In this work, we propose a novel multi-rate mass-transfer (MRMT) model for two-phase flow, which accounts for viscous-dominated flow in the fracture domain and capillary flow in the matrix domain. It extends the classical (i.e., single-rate) dual-porosity model to allow us to simulate the wide range of transfer rates occurring in naturally fractured multiporosity rocks. We demonstrate, by use of numerical simulations of waterflooding in naturally fractured rock masses at the gridblock scale, that our MRMT model matches the observed recovery curves more accurately compared with the classical dual-porosity model. We further discuss how our multi-rate dual-porosity model can be parameterized in a predictive manner and how the model could be used to complement traditional commercial reservoir-simulation workflows.

## Introduction

A major part of the world's remaining oil reserves is in naturally fractured reservoirs (NFRs), yet production from NFRs is often challenging—they suffer from a low final recovery that leaves 80 to 95% of the oil underground, retained in the low-permeability rock matrix (Kazemi and Gilman 1993). The classical way to model production from NFRs is the dual-porosity model (Warren and Root 1963) with its extension to multiphase flow (Kazemi et al. 1976; Gilman and Kazemi 1983, 1988; Quandalle and Sabathier 1989), which separates the reservoir into a flowing domain (the network of connected and permeable fractures) and a stagnant domain (the low-permeability rock matrix), with the latter providing the storage. The equivalent fracture permeability is usually computed from stochastically generated discrete fracture networks (DFNs), whereas the permeability of the rock matrix comes from plug measurements (Dershowitz et al. 2000; Bourbiaux et al. 2002; Garcia et al. 2007). The exchange of oil, gas, and water between the two domains is modeled by transfer func-

tions (describing the physics of fluid exchange between fracture and matrix) and a shape factor (describing the geometry of the rock matrix). Much research has been dedicated to the appropriate use of transfer functions (Abushaikh and Gosselin 2008; Lu et al. 2008; Al-Kobaisi et al. 2009; Babadagli et al. 2009; Balogun et al. 2009; Ramirez et al. 2009) and shape factors (Lim and Aziz 1995; Hassanzadeh and Pooladi-Darvish 2006; Rangel-German and Kovscek 2006; Gong et al. 2008), whereas scaling groups have been developed to quantify the rate of oil recovery from matrix blocks and its dependence on rock and fluid properties (Ma et al. 1997; Tavassoli et al. 2005; Mason et al. 2010; Schmid and Geiger 2012).

One fundamental concept in all dual-porosity models is that fluid exchange between fracture and matrix in each computational gridblock in a field-scale reservoir simulator can be described by a single transfer rate, the so-called “sugar cube model” (Warren and Root 1963), in which all matrix blocks within a computational gridblock have an identical shape and are assumed to be fully mixed (i.e., have a single averaged saturation).

In this case, the transfer rate is proportional to the difference of pressure or saturation in the continua, which is equivalent to a first-order rate model. These models lead typically to the equilibration of pressure or saturation differences with an exponential time behavior. The exchange of fluids is, however, mostly capillary driven. The dynamics of capillary flow is difficult to match with an exponential function (Schmid and Geiger 2012).

Yet, it is much more common that matrix blocks occur in various shapes and sizes in NFRs (Fig. 1a); thus, it may be more appropriate to use a distribution of shape factors in each gridblock (Fig. 1). Furthermore, the recovery rate resulting from counter-current imbibition depends strongly on the rock and fluid properties (Ma et al. 1997; Tavassoli et al. 2005; Mason et al. 2010; Schmid and Geiger 2012); thus, full mixing and uniform saturations in the matrix cannot be assumed. It is well known that the assumption of a uniform matrix property (e.g., pressure, saturation) underpredicts the early-time transfer of the oil from the matrix (Zimmerman et al. 1993). How long the “early” time is depends on the size and permeability of the matrix block because larger matrix blocks, which hold most of the oil, generally have larger “early” times; the resulting error for field-scale recovery can be large, which will be shown in the following. Small variations in matrix permeability and wettability also lead to nonequilibrium and incomplete mixing, which can manifest in different transfer rates; again, it may be more appropriate to capture this behavior through a distribution of transfer functions with different relative permeability and capillary pressure functions in each gridblock.

In the groundwater literature, a highly successful and natural extension of the classical dual-porosity model (here, usually called “mobile/immobile” model) was postulated more than 15 years ago for single-phase miscible flow, the so-called “multi-rate mass transfer model” (MRMT) model (Haggerty and Gorelick 1995). Any mobile/immobile, dual-porosity, model with a given shape factor is a special case of the MRMT model. It is easy to combine different geometries for the immobile (i.e., matrix) zones in the MRMT model: Rather than a single transfer rate and capacity ratio between the immobile and mobile zones, the MRMT uses a single statistical distribution for rate coefficients

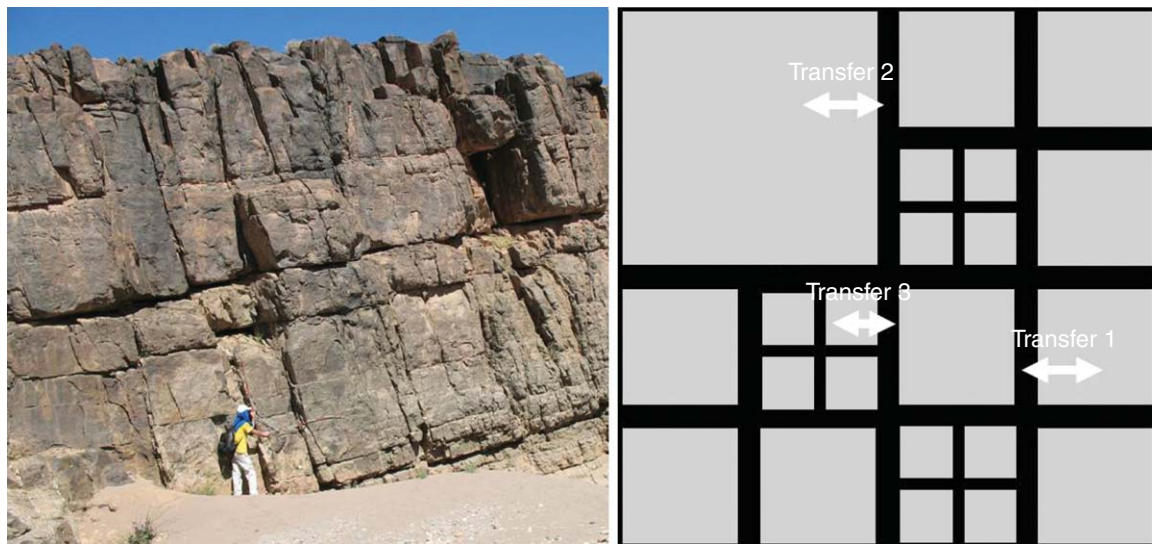


**Fig. 1—Left: Outcrop of a fractured carbonate sequence in Morocco (Courtesy of Herman Boro, University of Amsterdam). Note the vastly different sizes in matrix blocks. Right: Conceptual picture of a multi-rate dual-porosity model in which each gridblock contains a number of transfer functions to capture the distribution in matrix blocks and corresponding shape factors. The black region represents the high-permeability fractures in which advection dominates, whereas the gray regions are the low-permeability matrix blocks.**

and capacity ratios, which can vary locally with the properties of the reservoir (e.g., matrix-block size).

The MRMT model can be derived in different ways. In the most common formulation, one transport equation for the concentration in the mobile fracture system is solved, and the mass exchange with the matrix system is captured in a source/sink term that is nonlocal in time. The parameter that includes subscale structure shapes and process parameters in the immobile zone (i.e., matrix) is the memory function, which is the kernel of the nonlocal source/sink term. One could argue that it is inevitable that tracer-breakthrough curves can be fitted better with an MRMT model than with a single-rate model because the former has more fitting parameters. However, the parameters describing the memory function have a physical interpretation and can, in principle, be derived if the geometry and parameters of the substructure and the flow and transport processes in the continua are known in detail (Gouze et al. 2008a,b). This means that, in turn, information about substructure can be inferred from the parameters describing the memory function.

The MRMT model has been applied convincingly to interpret single- and multiple-well tracer tests in fractured dolomites in which it clearly outperformed the standard single-rate model (Haggerty et al. 2001; McKenna et al. 2001). In some wells, the single-rate dual-porosity model began to overpredict the recovery of the tracer after 20 hours by up to a factor 10. The MRMT model, on the other hand, provided a close match of the tracer recovery and demonstrated that the rate coefficients span up to 3.6 orders of magnitude. This had profound consequences on forecasting the large-scale transport behavior because the disequilibrium between the tracer concentration in the largest matrix blocks with the slowest rate coefficients and the concentration in the fractures prevailed for much longer times than predicted by a single-rate dual-porosity model. A similar behavior can be expected for oil recovery in which the largest matrix blocks, holding most of the oil, will have a heterogeneous distribution of oil and drain much slower and for much longer time scales than smaller matrix blocks. Also, oil drains because of capillary forces, which causes a different time behavior than a first-order process. The standard dual-porosity model can predict none of this. Yet, somewhat surprisingly, the MRMT model has not been used much in the reservoir-simulation and -engineering community. Only a single paper discusses its conceptual application to reservoir simulations by use of up to three instead of one first-order transfer rate, which results in significant variations in predicted

production rates because more geological heterogeneities can be included in the improved dual-porosity model (Di Donato et al. 2007).

Thus, the objective of this work is to provide a complete extension of the MRMT model to a two-phase flow in which fracture-matrix transfer is no longer first order and matrix saturations can be heterogeneous and can increase and decrease over time. We apply it to a high-resolution model of a world-class fractured reservoir outcrop analog, the Bristol Channel, UK (Belayneh 2004), which has been widely used to study single- and multiphase flows in fractured rock masses (Matthäi and Belayneh 2004; Belayneh et al. 2006, 2009; Geiger and Emmanuel 2010; Geiger et al. 2010); we compare results from direct high-resolution simulations of multiphase flow in the relevant fracture geometry with the classical single-rate and our new MRMT model. We illustrate, by use of idealized fracture geometries, how changes in the subscale geometry of the matrix blocks affect oil recovery, and we discuss how the MRMT model for multiphase flow could be parameterized by use of data from laboratory experiments and tracer tests.

In the next section, we review the key equations and introduce the MRMT model. This is followed by an illustrative example highlighting how changes in the distribution of matrix-block sizes affect oil recovery and, similarly, the breakthrough of a nonreactive tracer. We then apply the MRMT model to realistic fracture geometries exhibiting multiple transfer rates. We close by discussing our results and further possible extensions of the MRMT model. Note that in the following text we use the terms “MRMT model” and “multi-rate dual porosity” interchangeably, and, likewise, “single-rate mass transfer” and “classical dual-porosity model.”

## Mathematical Model and Numerical Solution

**Continuum Scale Modeling.** For continuum scale modeling (i.e., any simulations that model multiphase flow directly on high-resolution representations of the fracture geometries), we define an average pressure  $p$  (Chen et al. 2006) as follows:

$$p = p_o - \int_0^{S_w} \left( f_w \frac{dP_c}{dS_w} \right) d\xi, \quad \dots \dots \dots (1)$$

where  $S$  is the saturation,  $f$  is the fractional-flow function,  $P_c$  is the capillary pressure, and the subscripts  $w$  and  $o$  denote the water

and oil phase, respectively. The total fluid velocity  $v$  for both phases is then given as

$$v = -k(\lambda_t \nabla p) + (\lambda_w \rho_w + \lambda_o \rho_o) g \nabla z, \quad (2)$$

where  $k$  is the permeability (assumed to be a scalar for simplicity),  $\lambda_t = \lambda_w + \lambda_o$  is the total mobility of the oil and water phase,  $\rho$  is the fluid density, and  $z$  is the depth. Assuming incompressible fluids such that

$$\nabla \cdot v = q_w + q_o, \quad (3)$$

where  $q$  is the source/sink term for the oil or water phase, one can derive the elliptic equation describing the evolution of the average pressure field by inserting Eq. 2 into Eq. 3:

$$q_w + q_o = \nabla \cdot [k(\lambda_t \nabla p) + (\lambda_w \rho_w + \lambda_o \rho_o) g \nabla z]. \quad (4)$$

Mass balance for the saturation of the water phase  $S_w = 1 - S_o$  is given by

$$\phi \frac{\partial S_w}{\partial t} + \nabla \cdot (f_w v - D \nabla S_w + k_{fw} \lambda_o \Delta \rho g \nabla z) = 0. \quad (5)$$

Here,  $\phi$  is the porosity,  $\Delta \rho$  is the difference between the water and oil density ( $\Delta \rho = \rho_w - \rho_o$ ), and  $D$  is the nonlinear capillary diffusion coefficient given by

$$D = -k_{fw} \lambda_o \frac{dP_c}{dS_w}. \quad (6)$$

Note that, strictly speaking,  $D$  is a dispersion coefficient because it depends on  $S_w$ , which depends on  $v$ , but for consistency with matrix diffusion during miscible solute transport, we refer to it as “capillary diffusion coefficient.” Eq. 7 defines the fractional-flow function  $f_w$ ,

$$f_w = \frac{k_{r,w}/\mu_w}{k_{r,w}/\mu_w + k_{r,o}/\mu_o}. \quad (7)$$

We use the Corey model to compute the relative permeability  $k_r$  and use the Brooks-Corey model to compute the capillary pressure  $P_c$  for a water-wet matrix and fracture:

$$k_{ro} = \hat{S}_o \left( \frac{S_o - S_{or}}{1 - S_{or} - S_{wir}} \right)^\varepsilon, \quad k_{rw} = \hat{S}_w \left( \frac{S_w - S_{wir}}{1 - S_{or} - S_{wir}} \right)^\varepsilon, \\ P_c = P_d \left( \frac{S_w - S_{wir}}{1 - S_{or} - S_{wir}} \right)^{-1/\varepsilon}, \quad (8)$$

where  $\hat{S}$  is the endpoint saturation,  $S_{or}$  is the residual oil saturation,  $S_{wir}$  is the irreducible water saturation,  $P_d$  is the capillary entry pressure, and  $\varepsilon$  is an exponent normally adjusted to fit experimental data.

For miscible single-phase-flow simulations of a nonreactive tracer at constant fluid density, which we use to illustrate the similarities of miscible and immiscible fluid exchange between fracture and matrix and discuss possible calibration methods for the MRMT model, the equations simplify to

$$v = -\left(\frac{k}{\mu} \nabla p\right); \quad \nabla \cdot v = q, \quad (9)$$

where  $\mu$  is the fluid viscosity. Eq. 10 gives mass conservation of the concentration  $C$  of a nonreactive tracer:

$$\phi \frac{\partial C}{\partial t} + \nabla \cdot (vC - D_{1p} \nabla C) = 0, \quad (10)$$

where  $D_{1p}$  is the dispersion tensor, which is a function of the fluid velocity  $v$ , diffusion constant  $D$ , and longitudinal and transversal dispersion constants  $a_L$  and  $a_T$ , respectively (Bear 1972).

To generate a suite of reference data sets from well-controlled and carefully designed numerical experiments against which we

can test our MRMT model, we solve these equations by use of a combination of mixed-dimensional finite-element and finite-volume methods with semi-implicit timestepping for Eq. 5 in which the fractures are treated as  $d - 1$  elements (i.e., 1D line elements in 2D geometries and 2D surface elements in 3D geometries) (Geiger et al. 2004, 2009). For simplicity, we assume that the capillary entry pressure in fracture and matrix is identical in the direct numerical simulations, which allows us to overcome timestepping limitations for the case of discontinuous capillary pressures between the mobile and immobile domains (Reichenberger et al. 2006; Hoteit and Firoozabadi 2008) and thus to deal with more-complex and more geologically realistic fracture geometries. However, we note that our MRMT model does not require the assumption that the capillary entry pressure be continuous in fracture and matrix, as further discussed in the following, and we make this assumption only when numerically generating reference solutions. The algorithm is implemented in the “Complex System Modeling Platform” (CSMP++), an object-oriented simulation platform written in the C++ programming language that is tailor-made for high-resolution modeling of multiphase flow in geometrically complex porous media such as fractured rocks (Matthäi et al. 2007).

Note that the fractures in the Bristol Channel are layer bound, with individual layers only a couple of decimeters high (Belayneh 2004). Thus, we represent the Bristol Channel geometry, as well as the idealized fracture geometries, as 2D planar surfaces, and we neglect gravity terms in the preceding equations. Whereas this is a simplification of fracture-matrix transfer processes that occur in many NFRs in which gravitational forces can play an important role in oil recovery (Al-Kobaisi et al. 2009; Ramirez et al. 2009), it allows us to develop and validate our MRMT model step by step and to evaluate if our model can be applied for the limiting, but not unrealistic, case in which capillary forces dominate in the matrix. The extension to include gravitational forces is, in principle, possible and subject to our ongoing research, which will be discussed further later in the paper.

**MRMT Model.** The MRMT approach conceptualizes a heterogeneous medium as a multiple continuum medium consisting of a single mobile continuum and a distribution of immobile continua (Fig. 1). The immobile continua interact with the mobile continuum only by mass transfer over the domain interfaces (e.g., Haggerty and Gorelick 1995; Lichtner and Kang 2007). We first describe the MRMT model for solute transport and will extend it later for immiscible displacement.

**Solute Transport.** In the mobile domain, transport is advection-dominated, whereas in the immobile domain transport is caused only by diffusion and slow advection. Here we consider the case of diffusion only in the immobile regions. For transport in a fracture network, the mobile zones are identified with the fracture; the immobile zones are identified with the low-permeability matrix. The transport equation (Eq. 10) is formulated for each region with continuous concentration and solute flux at the interfaces between the mobile continuum and the immobile continua. Averaging over a support volume that contains a representative sample of the medium heterogeneity then leads to the following system of coupled equations. The concentration in the fracture  $C_f$  satisfies the nonlocal advection-dispersion equation (e.g., Carrera et al. 1998):

$$\phi_f \frac{\partial C_f}{\partial t} + \nabla \cdot (v_{\text{eff}} C_f - D_{\text{eff},1p} \nabla C_f) = -\frac{\partial}{\partial t} \int_0^t \phi(t - \tau) C_f(x, \tau) d\tau, \quad (11)$$

where  $\phi_f$  is the total fracture porosity. Here and in the following the subscript,  $f$  indicates that variables and parameters are considered in the mobile domain (the fracture system) only, whereas the subscript  $m$  denotes that variables and parameters are considered in the immobile matrix domain only. The macrodispersion coefficient  $D_{\text{eff},1p}$  reflects the spreading of the tracer plume resulting from velocity fluctuations in the mobile domain, and  $v_{\text{eff}}$  is the



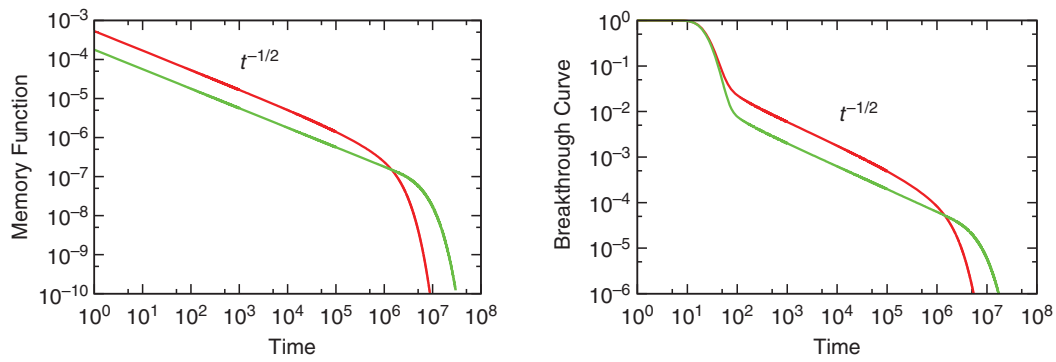


**Fig. 2—(Left) Memory function  $\phi(t)$  for diffusion into spheres (red) and into slabs (green) for the diffusion time  $\tau_d = 10^6$  s. (Right) Corresponding breakthrough curves for  $v_{\text{eff}} = 10^{-3} \text{ m}\cdot\text{s}^{-1}$ ,  $D_{\text{eff},1p} = 10^{-4} \text{ m}^2\cdot\text{s}^{-1}$ ,  $\tau_d = 10^{-7}$  seconds at a producer at  $x = 1 \text{ m}$ .**

spatially averaged transport velocity in the mobile domain times the volume fraction of the mobile domain, which could be obtained from upscaling flow in a DFN (Dershowitz et al. 2000). The right side of Eq. 11 is the time change of the averaged concentration in the immobile domain. The memory function  $\phi$  encodes the details of specific mass-transfer processes between mobile and immobile regions.

Here, we consider not only purely diffusive mass transfer between fracture and matrix but also purely diffusive transport within the matrix. The matrix is considered to be composed of blocks of different sizes. For this reason, the immobile matrix is considered an overlap of multiple immobile continua characterized by different characteristic sizes. To derive an expression for the memory function  $\phi$ , we consider the diffusion problem within a matrix block  $\Omega_i$  of typical size  $l_i$  described by

$$\phi_i \frac{\partial c_m^{(i)}}{\partial t} - D_{1p} \nabla_r^2 c_m^{(i)} = 0, \quad (12)$$

where  $\phi_i$  is the intrinsic matrix porosity. The exchange between fracture and matrix is described by the boundary condition in

$$c_m^{(i)} = C_f, r \in \Gamma_i, \quad (13)$$

where  $\Gamma_i$  is the interface between the mobile and the immobile domain and  $r$  is the position vector in the coordinate system attached to the matrix block. Note that  $c$  indicates the local concentration in the matrix, whereas  $C$  denotes the averaged concentration. We assume that the diffusion coefficient does not vary between different immobile regions. The immobile region of Type  $i$  can be characterized by the diffusion timescale  $\tau_{di} = l_i^2/D_{1p}$ . This boundary condition assumes that the scale of variability of the concentration in the fracture is much larger than the typical length scale  $l_i$  of the matrix blocks (e.g., the radius or distance from the matrix center to the nearest fracture). The immobile domains are, for simplicity, assumed to be initially solute free,  $c_m^{(i)}(r, t=0)=0$ , but this assumption is not an essential requirement for the MRMT model. The solution  $c^{(i)}(r, t)$  is expressed in

$$C_m^{(i)}(r, t) = \int_0^t dt' g(r, t-t'|\tau_{di}) C_f(x, t'), \quad (14)$$

where  $g(r, t|\tau_{di})$  is the Green function that is defined as the solution to the diffusion equation (Eq. 13) for the boundary condition  $g(r, t|\tau_{di}) = \delta(t)$  for  $r \in \Gamma_i$ . Thus, we use Eq. 15 to express the average concentration in  $\Omega_i$ :

$$C_m^{(i)}(x, t) = \int_0^t dt' \phi_i(t-t'|\tau_{di}) C_f(x, t'), \quad (15)$$

in which we defined the local memory function by

$$\phi_i(t|\tau_{di}) = \frac{1}{V_i} \int dr g(r, t|\tau_{di}). \quad (16)$$

In Eq. 17, the total immobile solute concentration is the weighted sum of the  $c_m^{(i)}$ ,

$$C_m(x, t) = \int_0^t dt' \phi(t-t') C_f(x, t'), \quad (17)$$

in which we defined the global memory function by

$$\phi(t) = \sum_i \pi_i \phi_i(t|\tau_{di}), \quad (18)$$

where  $\pi_i$  is the frequency of occurrence of immobile zones of Type  $i$ . The total porosity of the immobile zone is  $\phi_i = \phi_m \chi_i$  ( $\chi_i$  being the volume fraction of the immobile zone of Type  $i$ ). The total matrix porosity is  $\phi_m = \sum_i \pi_i \phi_i$ .

For 1D diffusion into slabs, the local memory function  $\phi_i(t)$  reads in Laplace space as (Harvey and Gorelick 1995)

$$\phi_i^*(\lambda) = \sqrt{\frac{1}{\lambda \tau_{di}}} \tanh(\sqrt{\lambda \tau_{di}}). \quad (19)$$

The asterisk denotes the Laplace-transformed memory function, and  $\lambda$  is the Laplace variable.

For diffusion into disks, the memory function appears as (Harvey and Gorelick 1995)

$$\phi_i^*(\lambda) = \frac{2}{\sqrt{\lambda \tau_{di}}} \frac{I_1 \sqrt{\lambda \tau_{di}}}{I_0 \sqrt{\lambda \tau_{di}}}, \quad (20)$$

where  $I_n(x)$  is the modified Bessel function of the first kind (Abramowitz and Stegun 1972).

For diffusion into spheres, the memory function is given by (Harvey and Gorelick 1995)

$$\phi_i^*(\lambda) = \frac{3}{\sqrt{\lambda \tau_{di}}} \left[ \coth(\sqrt{\lambda \tau_{di}}) - \sqrt{\frac{1}{\lambda \tau_{di}}} \right]. \quad (21)$$

The characteristic diffusion time in the immobile zone  $\tau_{di}$  represents the cutoff time when diffusion in the rock matrix stops (e.g., when the diffusion front reaches the boundary of the matrix block or multiple diffusion fronts meet at the center of the matrix block). Thus, for times much smaller than  $\tau_{di}$ , the memory function shows a  $t^{-1/2}$  behavior characteristic for diffusion, whereas for times larger than  $\tau_{di}$ , it decays exponentially fast, causing diffusion to terminate (Fig. 2). For diffusive mass transfer between fracture and matrix consisting of a single block type, the corresponding breakthrough curves for an initially uniformly distributed solute decrease as  $t^{-1/2}$  until they are cut off at the characteristic diffusion time  $\tau_d$  (Fig. 2).

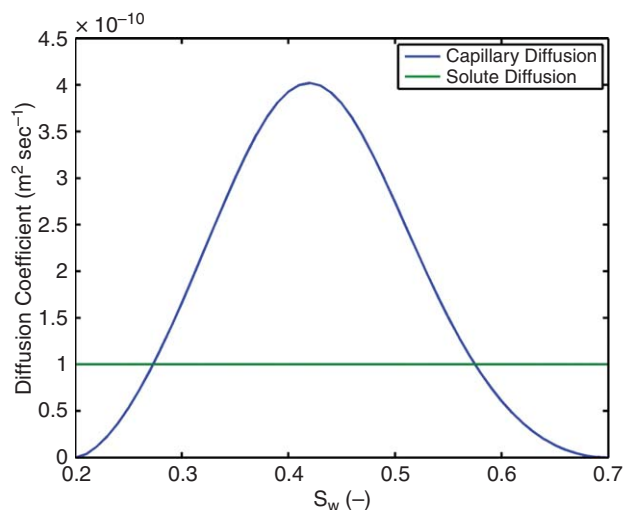


**Fig. 3—Capillary flow parameter (Eq. 6) and solute diffusion coefficient for the matrix in the test example (Table 1).**

Unlike single-rate first-order mass transfer, the diffusive mass-transfer model presented previously does not treat the immobile zone as fully mixed for times that are smaller than the typical diffusion timescale. This concept is comparable with the multiple interacting continua extension of the classical dual-porosity model (Pruess and Narasimhan 1985; Karimi-Fard et al. 2006; Gong et al. 2008; Tatomir et al. 2011), which also allows for local variations in saturation or concentration in the matrix. Diffusive mass transfer can be represented in terms of a first-order mass-transfer model by a distribution of transfer rates (Haggerty and Gorelick 1995; Carrera et al. 1998), that is, by a first-order MRMT model. Thus, in the following, we refer to this diffusive mass-transfer model also as the MRMT model. For linear first-order mass transfer between fracture and matrix, the memory function is given by an exponential,

$$\phi_i(t) = \alpha_i \exp(-\alpha_i t), \quad (22)$$

where the mass-transfer rate is  $\alpha_i$ . Explicit analytical solutions of Eq. 11 can be obtained in Laplace space for constant velocity and diffusion in the fracture. The time/space solutions are evaluated by the numerical inverse Laplace transform of these explicit expressions.

**Two-Phase Flow.** A similar multicontinuum approach can be applied to the two-phase-flow problem (Eq. 5), in which the displacing fluid is transported in the mobile domain by viscous and gravity forces mainly and in the immobile domain by capillary forces only. Fracture and matrix communicate by way of the interface, for which we impose the standard condition that capillary pressure and total flux are continuous. This implies that saturations are discontinuous at the interface if the capillary entry pressure is discontinuous in fracture and matrix, which commonly is the case for fractured porous media. Because we impose only flux and pressure continuity and not saturation continuity in our MRMT model, this situation is automatically accounted for. However, because our numerical reference solutions assume, for simplicity, that the capillary entry pressure is identical in fracture and matrix, the continuity of pressure implies the continuity of saturation in this specialized case.

In contrast to the single-phase solute transport case discussed previously, the flow equation in the immobile domain is now nonlinear because capillary-driven spontaneous counter-current imbibition is a nonlinear diffusion process. Note that we use spontaneous counter-current imbibition and nonlinear diffusion interchangeably. Here, we argue that spontaneous counter-current imbibition is similar to diffusion when looking only at the time behavior of the average fluid content in the matrix, which in the MRMT approach is the relevant observable. The actual fluid distribution in the immobile domain is not needed in the MRMT frame-

work. Thus, analogous to the MRMT model for solute transport, the water saturation in the fracture satisfies the following equation:

$$\phi_f \frac{\partial S_{wf}}{\partial t} + \nabla \cdot [f_{wf} v_{\text{eff}} + D_f \nabla S_{wf} + (k f_w \lambda_o)_f \Delta \rho g \nabla z] = - \frac{\partial}{\partial t} \int_0^t \mu(t - \tau) S_{wf}(x, \tau) d\tau. \quad (23)$$

The total flux  $v_{\text{eff}}$  is the spatial average of the total flux in the mobile domain. The term on the right-hand side quantifies the fluid exchange between fracture and matrix; the memory function for the flow problem is denoted by  $\mu(t)$ . The model given by Eq. 23 is no longer an exact solution of the full flow problem, because the convolution with the memory function solves only linear problems. Nevertheless, we argue that the similarity of the time behavior of capillary counter-current flow and diffusion and the fact that the detailed saturation distribution in the matrix is not needed for the mass exchange justify this approach.

Fluid transfer between fracture and matrix and flow in the matrix is caused by capillary diffusion only. The capillary flow equation in the immobile domain of Type  $i$  then is given by

$$\phi_i \frac{\partial S_{wi}}{\partial t} - D_{mi} \nabla_r^2 S_{wi} = 0 \quad (24)$$

with the boundary condition

$$P_{ci}(S_{wi}) = P_{cf}(S_{wf}) \text{ on } \Gamma_i. \quad (25)$$

As previously mentioned,  $s$  denotes the local saturation in the matrix. It is assumed that initially there is no water in the matrix,  $S_{wi}(r, t=0) = 0$ . This assumption is used for simplicity, but it could be relaxed because the connate-water saturation rarely will be zero in real applications. The constant capillary diffusivity  $D_{mi}$  in the matrix is approximated as the average over the capillary diffusivity  $D_{mi}(S_{wi}) = k_{r,mifwi} \lambda_o (dP_c/dS_{wi})$  for different water saturations (Fig. 3). The actual value of a constant  $D_{mi}$  can be estimated by computing the appropriate scaling group for a given laboratory imbibition experiment because the scaling group always contains the information needed to compute the full nonlinear diffusion coefficient  $D_{mi}(S_{wi})$  (Schmid and Geiger 2012). With this approximation, the immobile flow problem is mathematically equivalent to the diffusion problem (Eq. 12) in the matrix. The capillary diffusion timescale,  $\tau_{ci} = l_i^2/D_{mi}$ , characterizes flow in the immobile zone of Type  $i$  and, analogous to  $\tau_{di}$ , defines the cutoff time as the time when diffusion resulting from spontaneous counter-current imbibition in the matrix stops. Similar to  $\tau_{di}$ , it can be estimated by defining a characteristic length scale  $l_i$  and the average constant capillary diffusivity  $D_{mi}$ . The  $\tau_{ci}$  also can be computed accurately from imbibition experiments with the appropriate scaling group to compute the time when the wetting front reaches the nearest boundary or center (in case of multiple invading wetting fronts) of a matrix block (Schmid and Geiger 2012). The global memory function is thus given by

$$\mu(t) = \sum_i \pi_i \phi_i(t|\tau_{ci}). \quad (26)$$

The local memory functions  $\phi_i(t|\tau_{ci})$  are given by Eq. 16. In this approximation, the only difference between the local memory for flow and solute transport is the diffusion timescales  $\tau_{di}$  and  $\tau_{ci}$ . Thus, in principle, the memory function  $\mu(t)$  for the two-phase-flow problem can be obtained from the one for solute transport by rescaling the diffusion timescales although there may be practical issues, depending on the wettability of the rock and the particular shape of the relative permeability and capillary pressure curves. For example, in mixed-wet systems, spontaneous imbibition occurs only when the capillary pressure is larger than zero. The rate of spontaneous imbibition also decreases with increasing oil-wetness in mixed-wet systems (Behbahani and Blunt 2005). It must be explored how the diffusion timescales need to be rescaled in such situations, but this can be achieved, in principle, without

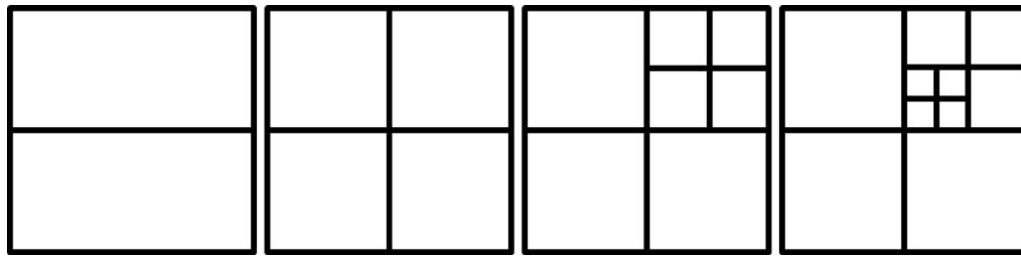


**Fig. 4—Map view of four idealized 2D fracture patterns containing (from left to right) 1, 2, 4, and 6 fractures and thus successively smaller matrix geometries blocks. These geometries are used to illustrate how simple variations in fracture geometry affect recovery and solute/saturation distributions in the matrix blocks, as well as to highlight similarities between miscible solute transport and immiscible two-phase flow. Dimensions of all models are 1 × 1 m. A horizontal injector is at the left model boundary, injecting water at a constant rate ( $q_w = 10^{-5} \text{ m}^3 \cdot \text{m}^{-2} \cdot \text{s}^{-1}$ ), whereas a horizontal producer is at the right boundary, producing at a fixed bottom-hole pressure ( $10^7 \text{ Pa}$ ). The top and bottom boundaries are no-flow boundaries. The geometries are discretized by approximately 6,800 finite elements and 3,225 finite volumes with local grid refinement around the fractures to model the initially steep concentration and saturation gradients between fracture and matrix accurately. The timestep was 0.005 days to minimize numerical errors resulting from a coarse temporal discretization.**

need for further numerical simulations with the appropriate scaling group (Schmid and Geiger 2012).

For completeness, we point out that our proposed model for two-phase flow has some similarities to the discrete dual-porosity model by Di Donato et al. (2007) that uses a distribution of first-order transfer functions to describe mass exchange between fracture and matrix:

$$\phi_f \frac{\partial S_{wf}}{\partial t} + \nabla \cdot (D \nabla S_{wf} + f_w v) = - \sum_{i=1}^n T_i, \quad \dots \quad (27)$$

with the first-order transfer functions

$$T_i = \phi_{m,i} \frac{\partial S_{wm,i}}{\partial t} = \beta_i (\tilde{S}_{wm,i} - S_{wm,i}), \quad \dots \quad (28)$$

where  $S_{wm,i}$  is the water saturation in the  $i$ th matrix block with porosity  $\phi_{m,i}$ ,  $\tilde{S}_{wm,i}$  is the water saturation after imbibition in the same matrix block, and  $\beta_i$  is the rate coefficient in Matrix Block  $i$ , which can be computed by an exact analytical solution or by empirical relations (Schmid and Geiger 2012). Finally, the following closure relations apply:

$$T = \sum_{i=1}^n T_i, \quad \phi_m = \sum_{i=1}^n \phi_{m,i}, \quad \phi_m S_{wm} = \sum_{i=1}^n \phi_{m,i} S_{wm,i}. \quad \dots \quad (29)$$

However, our MRMT model (Eq. 23) differs from the dual-porosity model by Di Donato et al. (2007) in several ways: First, it is nonlocal in time (i.e., the exchange of mass between matrix and fracture at one moment influences the mass in the fracture also at later times). In the transfer-function approach (Eq. 27), mass transfer stops when the saturation in the matrix is zero ( $T_i = 0$  if  $S_{wm,i} = \tilde{S}_{wm,i}$ ), which is a good approximation for plug-like displacement. In addition, the transfer function (Eq. 28) allows only for the transport of oil from the matrix into the fracture because  $T$  depends on the matrix saturation and not on the fracture and matrix saturation. In our MRMT model (Eq. 23), neither of the two is the case. Mass can be transferred to the fracture even after a pulse of displacing fluid has passed through (e.g., during alternating injections of water and gas), and the oil saturation in the matrix can increase and decrease. Furthermore, in standard models that describe mass transfer as proportional to differences of saturations or pressures, such as in Eq. 28, the stagnant continuum (here, the matrix) is considered as a fully mixed system. Transport inside of the immobile domain is not reflected. In the MRMT model (Eq. 23), diffusive or capillary transport in the stagnant continuum is reflected in the memory function. Specifically, the matrix is not treated as a fully mixed system. Only for times that are large compared with the typical diffusion timescale can it be treated as such.

## Direct Numerical Simulation

**Idealized Fracture Geometry.** We first illustrate the effect of fracture geometry and matrix-block-size distributions on production behavior during both miscible single-phase and immiscible two-phase flow with a set of idealized fracture geometries in a 1 × 1-m unit box (Fig. 4). Such runs also demonstrate that the rock matrix does not possess a uniform solute concentration or oil saturation when the time  $t$  is smaller than the diffusion timescale  $\tau_{di}$  in matrix block  $i$ . Parameters used for the single- and two-phase-flow simulations are given in Table 1. As mentioned previously, for simplicity, we use the same capillary entry pressure in fracture and matrix for the direct numerical solutions, but we reiterate that this is not a requirement for the MRMT model. Note that the viscosity ratio  $\mu_w/\mu_o = 0.2$  is applied to all two-phase-flow simulations. A horizontal injector injecting at a constant rate of  $q_w = 10^{-5} \text{ m}^3 \cdot \text{m}^{-2} \cdot \text{s}^{-1}$  is placed at the left model boundary, and a horizontal producer with a fixed bottomhole pressure of  $10^7 \text{ Pa}$  is placed at the right model boundary. In the two-phase case, water is injected; in the single-phase case, water is enriched with a nonreactive tracer.

Fig. 5 shows the evolution of the concentration field of the nonreactive tracer and the oil saturation for the different fracture geometries at 100 and 400 days. In all cases, the backbone of the fracture network is filled with the tracer, is filled with the tracer, respectively with the injected water, very fast. Breakthrough in the fracture backbone is not discussed further or illustrated. The

**TABLE 1—OVERVIEW OF PARAMETERS USED IN THE SIMULATIONS**

Parameter	Single Phase		Two Phase	
	Matrix	Fracture	Matrix	Fracture
$k$ (md)	1.0	$8.3 \times 10^7$	1.0	$8.3 \times 10^7$
$\phi$	0.25	1.0	0.25	0.1
$P_d$ (Pa)	—	—	$2.5 \times 10^4$	$2.5 \times 10^4$
$\varepsilon$ for $k_{ro}$	—	—	2.0	1.0
$\varepsilon$ for $k_{rw}$	—	—	3.0	1.0
$\varepsilon$ for $Pe$	—	—	3.0	3.0
$S_{or}$	—	—	0.3	0.0
$S_{wir}$	—	—	0.2	0.0
$S_o$	—	—	0.7	0.7
$S_w$	—	—	0.3	0.3
$D$ ( $\text{m}^2 \cdot \text{s}^{-1}$ )	$10^{-10}$	$10^{-10}$	—	—
$a_L$ (m)	0.01	0.01	—	—
$a_T$ (m)	0.001	0.001	—	—

Note: Fracture permeabilities are computed by use of the parallel-plate law for a fracture aperture of 0.001 m. The initial oil saturation is uniform at  $S_o = 0.8$  in all models. Relative permeability and capillary pressure are modeled using the Corey and Brooks-Corey models, respectively, for water-wet rocks (Eq. 8).



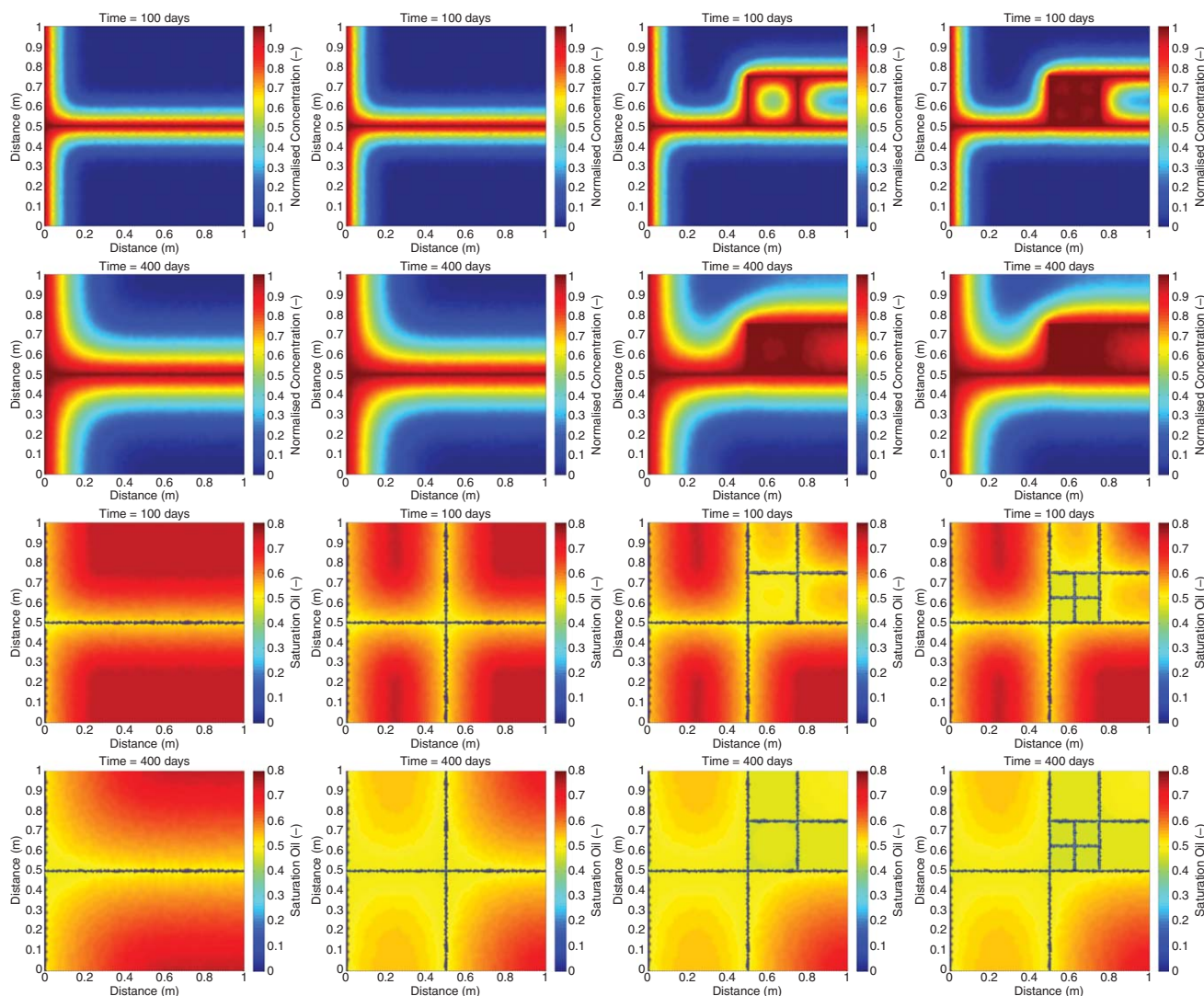
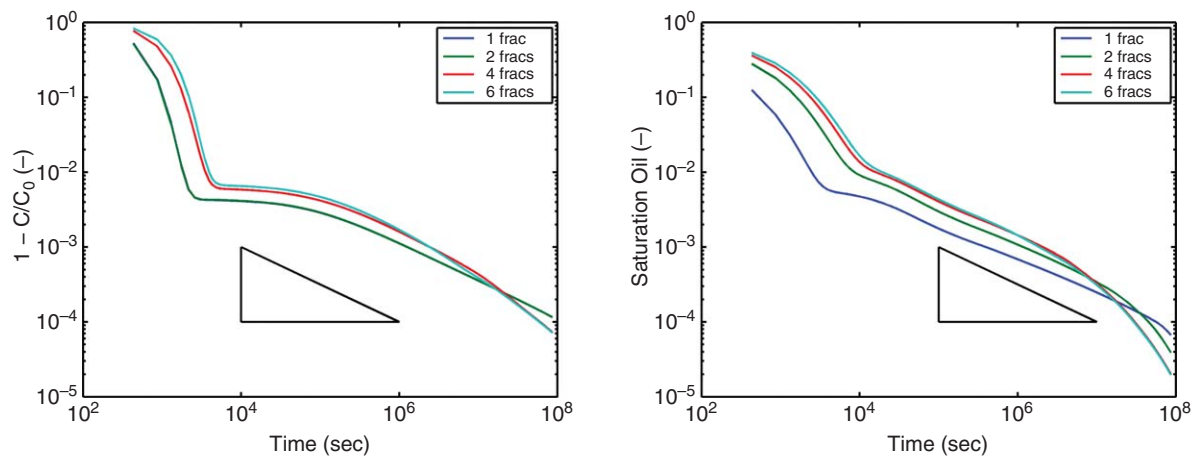


**Fig. 5—Map view of the concentration of a nonreactive tracer (top two rows) and oil-saturation (bottom two rows) distributions in the idealized fracture geometries (Fig. 4) at 100 and 400 days. It is clearly visible how the differently sized matrix blocks drain at different rates, both for the single-phase transport of a nonreactive tracer and for the immiscible two-phase transport, and that concentration and saturation distributions are nonuniform in the matrix. Note that capillary diffusion is much faster than solute diffusion in the fractures because the former scales with permeability (Eq. 6). Thus, water can enter the dead-end vertical fractures, whereas solute diffusion occurs at the same rates in vertical fractures and matrix.**

high tracer concentration, respectively high water saturation, presents the boundary condition for diffusion and counter-current imbibition that drive tracer and water into the low-permeability rock matrix. It is clearly visible how the differently sized matrix blocks drain at different rates and that the distribution of solutes, and their respective saturation, is nonuniform in each matrix block. Also, the patterns are similar for the miscible single-phase transport and immiscible two-phase case, which supports the idea that data from a tracer test could be used to calibrate the MRMT model for two-phase flow. However, there is one noticeable difference: Because capillary diffusion scales with the permeability (Eq. 6), this process is much faster than solute diffusion in the fractures. Thus, water enters the vertical fractures faster than the matrix even when the fractures are stagnant [i.e., the Darcy velocity is (close to) zero]. Solute diffusion, which is the only means to fill stagnant vertical fractures during tracer transport, occurs roughly at the same rates in the fractures and matrix. It is normally significantly slower than capillary diffusion. Thus, the stagnant vertical fractures are still solute free during tracer transport or have concentrations not discernibly different from those of the matrix. **Fig. 6** shows the breakthrough curves for the flux-weighted concentration of the nonreactive tracer and the oil saturation. The first part of the breakthrough curves, which shows an exponential decay in con-

centration, respectively saturation, corresponds to the advective transport in the backbone of the fractures. All curves show a similar behavior at late time (i.e., when transport and recovery are dominated by the slow diffusive exchange and counter-current imbibition between fracture and matrix), as is evident in the  $-1/2$  slope that is characteristic of the  $t^{-1/2}$  diffusion behavior (Fig. 2). However, the oil saturation does not follow the  $-1/2$  slope exactly, most likely because of the nonlinearity of the diffusion process (Eq. 6). The average tracer concentration, with respect to oil saturation, at the producer increases with the increasing number of fractures because the matrix blocks can be drained more efficiently. Departure from the  $t^{-1/2}$  behavior toward an exponential decay in concentration, respectively saturation, is visible for four and six fractures. Because these models have smaller matrix blocks, this behavior is likely caused because time  $t$  is larger than the characteristic diffusion time  $\tau_{di}$  in some matrix blocks (Fig. 2).

**Bristol Channel.** We now study and compare miscible single-phase flow and immiscible two-phase flow in the Bristol Channel, UK. The Bristol Channel is a world-class fractured reservoir outcrop analog in which layer-bound fractures, approximately 30 cm high, have formed in a limestone anticline (Belayneh 2004).



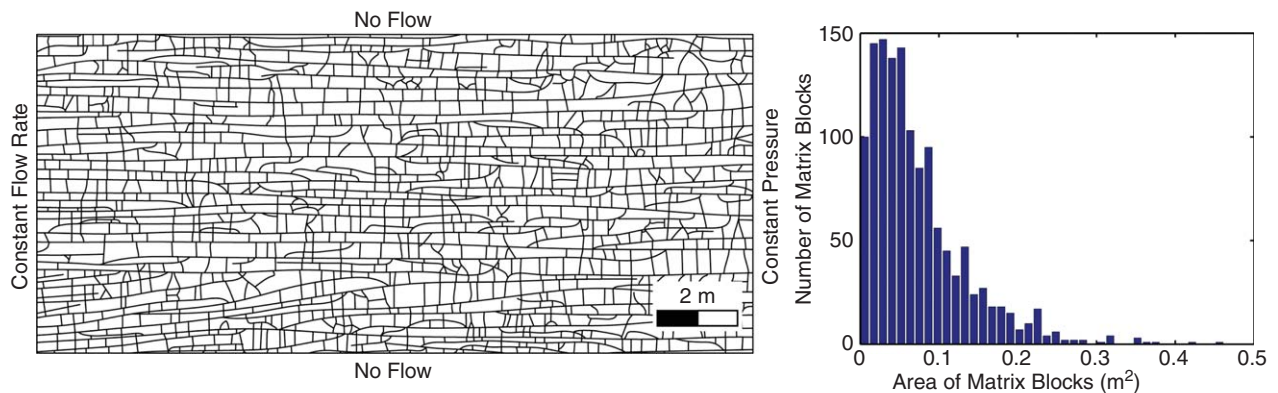
**Fig. 6—Breakthrough curves of the flux-weighted concentration of the nonreactive tracer (left) and oil saturation (right) at the producer at the right-side model boundary for the idealized fracture models (Fig. 4). The black triangle shows the  $-1/2$  slope typical for diffusion processes. Note the striking similarity between the concentration and solute breakthrough curves although the saturation breakthrough curve does not completely follow a  $-1/2$  slope, caused by the nonlinearity of the diffusion process.**

Fig. 7 shows the model geometry ( $18 \times 8 \text{ m}^2$  in size), which has been widely used to study single- and multiphase flow in fractured rock masses (Matthäi and Belayneh 2004; Belayneh et al. 2006, 2009; Geiger and Emmanuel 2010; Geiger et al. 2010). In contrast to the aforementioned idealized fracture pattern, the Bristol Channel fracture pattern comprises more than 1,000 highly irregular matrix blocks. Their size roughly follows a log-normal distribution (Fig. 7). As in the idealized fracture-pattern case, we inject water (containing a tracer in the single-phase case) at the left-side boundary through a horizontal injector operating at a constant rate, and we extract fluid at the right-side model boundary at the horizontal producer operating at a fixed bottomhole pressure. Here, however, we test two constant flow rates of  $q_w = 10^{-5} \text{ m}^3 \cdot \text{m}^{-2} \cdot \text{s}^{-1}$  and  $q_w = 10^{-4} \text{ m}^3 \cdot \text{m}^{-2} \cdot \text{s}^{-1}$ . As before, the producer operates at a fixed bottomhole pressure of  $10^7 \text{ Pa}$ . An analysis of the flow rates in the fractures and matrix shows that there is a distinct separation in fluid velocities, indicative of a dual-porosity behavior; flow rates in the fractures are between  $10^{-5}$  and  $10^{-2} \text{ m} \cdot \text{s}^{-1}$ , whereas they are approximately  $10^{-9} \text{ m} \cdot \text{s}^{-1}$  in the matrix (Geiger et al. 2010).

Fig. 8 shows the distribution of concentration and oil saturation in the Bristol Channel model. As in the simple fracture geometries (Fig. 5), the fractures are immediately filled with tracer, respectively water, whereas the exchange of tracer and water between fractures and matrix caused by diffusion, respectively

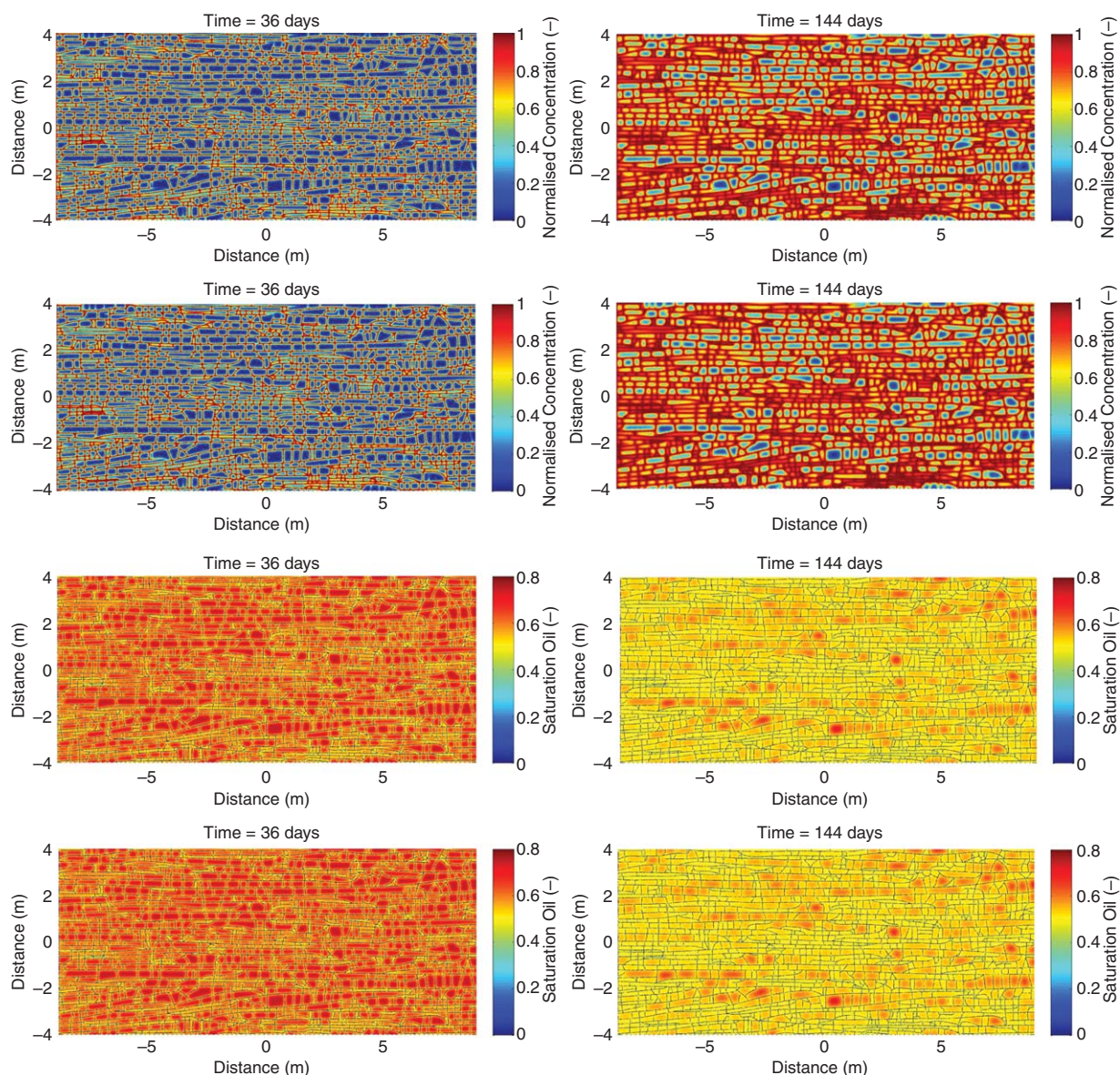
counter-current imbibition, occurs at much slower rates. Again, there are striking similarities between the concentration and saturation distributions, which show how the larger matrix blocks are saturated with tracer and water at a much slower rate than the smaller matrix blocks; consequently, the larger matrix blocks have heterogeneous concentration and saturation distributions for much longer timescales. The similarity between the concentration and saturation distributions in the matrix is to be expected because in both cases the mass transfer between fracture and matrix is driven by diffusion (Eqs. 12 and 24). However, no apparent difference in the tracer and saturation distributions prevails between the two different flow rates of  $q_w = 10^{-5} \text{ m}^3 \cdot \text{m}^{-2} \cdot \text{s}^{-1}$  and  $q_w = 10^{-4} \text{ m}^3 \cdot \text{m}^{-2} \cdot \text{s}^{-1}$ . This is because transport in the fractures is affected predominantly by the flow rates; after the high concentrations, respectively water saturations, are established in the fractures, they serve as boundary conditions for the diffusive exchange of tracer and counter-current imbibition of water between fracture and matrix.

Fig. 9 shows the breakthrough curves for the nonreactive tracer and the oil saturation at the producer at the right-side model boundary. Contrary to the idealized fracture patterns (Fig. 6), the curves differ between tracer transport and two-phase flow. Breakthrough of the tracer (Fig. 9, left) does not exhibit the typical power-law behavior at late time with a  $-1/2$  slope; instead, it shows another decaying exponential. Geiger et al. (2010)



**Fig. 7—Map of the Bristol Channel fracture geometry (left) and statistical distribution of the matrix-block sizes (right). Model dimensions are  $18 \times 8 \text{ m}^2$ . A horizontal injector is at the left-side model boundary, injecting water at a constant rate ( $q_w = 10^{-5} \text{ m}^3 \cdot \text{m}^{-2} \cdot \text{s}^{-1}$  or  $q_w = 10^{-4} \text{ m}^3 \cdot \text{m}^{-2} \cdot \text{s}^{-1}$ ), whereas a horizontal producer is at the right-side boundary, producing at a fixed bottomhole pressure ( $10^7 \text{ Pa}$ ). The top and bottom boundaries are no-flow boundaries. The geometries are discretized by approximately 351,000 finite elements and 155,000 finite volumes. Finite elements and finite volumes are unstructured, to discretize the curved and intersecting fractures accurately. The grid is locally refined around the fractures to model the initially steep concentration and saturation gradients between fracture and matrix accurately; the smallest finite elements, in the fractures, have an area of less than  $1 \text{ mm}^2$ . The timestep was 0.005 days, to minimize numerical errors caused by a coarse temporal discretization.**





**Fig. 8—Map view of the concentration of a nonreactive tracer (top two rows) and oil-saturation (bottom two rows) distributions in the Bristol model (Fig. 7) at 36 and 144 days. The first row of the concentration, respectively saturation, distribution, corresponds to an injection rate of  $q_w = 10^{-5} \text{ m}^3 \cdot \text{m}^{-2} \cdot \text{s}^{-1}$  whereas the second row corresponds to an injection rate of  $q_w = 10^{-4} \text{ m}^3 \cdot \text{m}^{-2} \cdot \text{s}^{-1}$ . As in the idealized fracture geometry, it is clearly visible how the differently sized matrix blocks drain at different rates, both for the single-phase transport of a nonreactive tracer and for the immiscible two-phase transport.**

interpreted this behavior as a superposition of three decaying exponentials, one belonging to transport in the fractures, another one to transport in the matrix, and the last one to fracture-matrix exchange. Haggerty et al. (2001) discussed that this behavior (i.e., exponential decay at late time) may arise in fractured porous media if there is sufficient heterogeneity in the advective regime and drift of tracer particles between slow- and fast-flowing regions. The transport velocities in the fractures vary more than three orders of magnitude in this case; consequently, heterogeneity in the flow field and drift may cause the exponential decay at late time. All breakthrough curves are shifted to earlier times for the higher flow rates of  $q_w = 10^{-4} \text{ m}^3 \cdot \text{m}^{-2} \cdot \text{s}^{-1}$  simply because breakthrough in the fractures occurs earlier and the boundary conditions for fracture-matrix exchange are established earlier. Breakthrough curves for the oil saturation (Fig. 9, right) show a  $t^{-1/2}$  behavior, while  $t < \tau_c$  and then shifts to a decaying exponential. At low flow rates of  $q_w = 10^{-5} \text{ m}^3 \cdot \text{m}^{-2} \cdot \text{s}^{-1}$ , the transition between early advective transport in the fractures and late fracture-matrix exchange caused by counter-current imbibition is not as obvious in the saturation curve although the transition to a

decaying exponential at very late time is more pronounced and occurs at approximately the same time as for the high flow rate of  $q_w = 10^{-4} \text{ m}^3 \cdot \text{m}^{-2} \cdot \text{s}^{-1}$ . We interpret this behavior as follows: At low flow rates, the advective transport of oil in the fractures is less efficient. Thus, the oil saturation in the fractures remains at a slightly higher value, which, in turn, reduces the rate at which counter-current imbibition operates at early time because of the different boundary conditions (i.e., water saturations) around the matrix blocks. Both effects combine to cause the slower breakthrough of water at the producer, both in time and in the rate at which the oil saturation decreases. If there were no nonlinear feedback between advective transport in the fractures and counter-current-driven fluid exchange between fractures and matrix, then the oil-saturation breakthrough curves would simply be shifted in time as in the nonreactive-tracer case.

### Application of the MRMT Model

For the following application, we consider Eq. 23 in  $d = 1$  dimension. We approximate the fractional-flow function  $f_{wf}$  as a linear

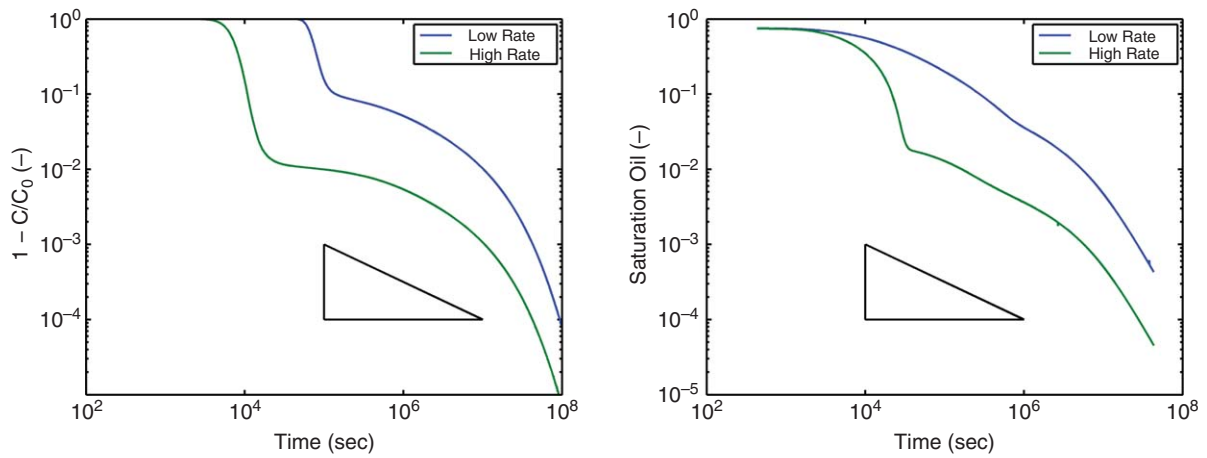


**Fig. 9—Breakthrough curves of the flux-weighted concentration of the nonreactive tracer (left) and oil saturation (right) at the producer at the right-side model boundary for the Bristol model (Fig. 7a). The black triangle shows the  $-1/2$  slope typical for diffusion processes. Note the similarity between the concentration and solute breakthrough curves at high flow rates. Note that the breakthrough curves for the nonreactive tracer do not follow a  $-1/2$  slope, whereas one of the breakthrough curves for the oil saturation is parallel to a  $-1/2$  slope.**

function of the saturation, and we assume that the capillary diffusion coefficient  $D_f$  does not depend on saturation. The reasoning for this simplification is that flow in the fracture is viscous-dominated flow, leading to a sharp displacement front, which can be approximated by a piston-type displacement. Gravity is disregarded in the aforementioned numerical example. Thus, the two-phase-flow problem essentially reduces to a transport problem for a nonreactive tracer (Eq. 11), and Eq. 23 reads as the following:

$$\phi_f \frac{\partial S_{wf}}{\partial t} + \frac{\partial}{\partial x} \left( v_{\text{eff}} - D_f \frac{\partial S_{wf}}{\partial x} \right) = - \frac{\partial}{\partial t} \int_0^t \mu(t - \tau) S_{wf}(x, \tau) d\tau. \quad (30)$$

For a boundary condition, we specify a step input into the fracture at the inlet at  $x=0$  and zero saturation gradient at the outlet at  $x=L$ ,

$$S_{wf}(x=0, t) = S_{wf,0} \Theta(t), \quad \left. \frac{\partial S_{wf}(x)}{\partial x} \right|_{x=L} = 0, \quad (31)$$

where  $\Theta(t)$  denotes the Heaviside step function and  $S_{wf,0}$  is the water saturation at the boundary. The initial water saturation is set to zero,  $S_{wf}(x, t=0) = 0$ . A solution for this initial-boundary-value problem can be conveniently obtained in Laplace space. The Laplace transform of Eq. 30 in time gives

$$\phi_f \lambda S_{wf}^* + \frac{\partial}{\partial x} \left( v_{\text{eff}} - D_f \frac{\partial S_{wf}^*}{\partial x} \right) = - \lambda \mu^* S_{wf}^*, \quad (32)$$

where  $S_{wf}^*$  denotes the Laplace transform of  $S_{wf}$  and  $\lambda$  denotes the Laplace variable. The boundary condition (Eq. 31) at the inlet transforms as  $S_{wf}^* = \lambda^{-1} S_{wf,0}$ ; the one at the outlet remains unchanged. The solution of Eq. 32 can be obtained by an exponential Ansatz. In this way, we obtain the explicit Laplace-space solution

$$S_{wf}^* = \exp[A_-(\lambda)] - \frac{A_-(\lambda) \exp[A_-(\lambda)L]}{A_-(\lambda) \exp[A_-(\lambda)L] - A_+(\lambda) \exp[A_+(\lambda)L]} \{ \exp[A_-(\lambda)x] - \exp[A_+(\lambda)x] \}, \quad (33)$$

$$\text{where } A_{\pm}(\lambda) = \frac{v_{\text{eff}}}{2D_f} \pm \sqrt{\frac{v_{\text{eff}}^2}{4D_f^2} + \frac{\lambda[\phi_f + \mu^*(\lambda)]}{D_f}}. \quad (34)$$

The solution in time/space is obtained by the Laplace inversion of this expression. The inverse Laplace transform is performed numerically with the free software package Octave (Eaton et al. 2011).

The volume fraction of the fracture domain for the Bristol model is  $\chi_f \approx 0.01$ . Thus, we set the total fracture porosity to  $\phi_f \approx 0.01$ . The volume fraction of the matrix domain is  $\chi_m \approx 1$ , and thus, the total matrix porosity is essentially equal to the intrinsic matrix porosity  $\phi_m = 0.25$  (Table 1). The effective velocity is set equal to the applied flow rates,  $v_{\text{eff}} = q_w$ . The fracture dispersion coefficient is adjusted from the high-flow-rate data set ( $q_w = 10^{-4} \text{ m} \cdot \text{s}^{-1}$ ) to  $D_f = 5 \times 10^{-4} \text{ m}^2 \cdot \text{s}^{-1}$ . Note that  $D_f$  represents a macroscopic dispersion coefficient that results from the velocity contrasts in the fracture network and therefore is proportional to the flow rate. Thus, for the low-flow-rate data set ( $q_w = 10^{-5} \text{ m} \cdot \text{s}^{-1}$ ), we set the dispersion coefficient in the fracture to  $D_f = 5 \times 10^{-5} \text{ m}^2 \cdot \text{s}^{-1}$  (i.e., one order of magnitude smaller than for the high-flow-rate case).

As mentioned previously, the typical diffusion timescale  $\tau_{c,i}$  is directly proportional to the size of the Matrix Block  $i$ . If there is a distribution of matrix-block sizes for a given geometry such as the Bristol Channel model (Fig. 7), one can thus expect a distribution of typical diffusion timescales. However, the distribution of block sizes in the Bristol Channel geometry is characterized by a well-defined peak at small values of approximately  $10^{-2} \text{ m}^2$ . Thus, for simplicity, we represent the matrix as consisting of a single block type with a typical area of the order of  $10^{-2} \text{ m}^2$ . This gives a typical diffusion time of  $\tau_c \approx 10^7$  seconds. As outlined previously, the mass-transfer model used here (namely, diffusive mass transfer between fracture and a single matrix-block type) corresponds to an MRMT model with distributed linear first-order mass-transfer rates (Haggerty and Gorelick 1995; Carrera et al. 1998). We use three types of memory functions that approximate the geometry of matrix blocks as spheres (Eq. 21), as disks (Eq. 20), and as slabs (Eq. 19), with appropriate adjustment of the characteristic diffusion time  $\tau_c$ . The characteristic timescale  $\tau_c$  for diffusion into spheres is adjusted to  $\tau_c = 9 \times 10^7$  seconds, for diffusion into disks to  $\tau_c = 5 \times 10^7$  seconds, and for diffusion into slabs to  $\tau_c = 1.5 \times 10^7$  seconds. For comparison, we also consider a classical first-order single-rate model [i.e., a standard dual-porosity model (Eq. 22)] for which a characteristic rate of  $\alpha = 2 \times 10^{-7} \text{ s}^{-1}$  is adjusted. The oil saturation is obtained for the water saturation  $S_{wf}$  as  $S_{of} = S_{wf,0} - S_{wf}$ . The producer is at a distance of 18 m from the injection well at the right-side domain boundary. Thus, in the previous solution Eq. 33, we set  $x = L = 18 \text{ m}$ .

**Fig. 10** shows the simulated breakthrough curves for the oil saturation at the producer for a high flow rate of  $q = 10^{-4} \text{ m}^3 \cdot \text{m}^{-2} \cdot \text{s}^{-1}$  and the corresponding results from the MRMT models described previously and the classical dual-porosity (single-rate) model. Excellent agreement for the late-time behavior (i.e., the production behavior that is dominated by counter-current imbibition after water breakthrough occurred in the fractures) can be

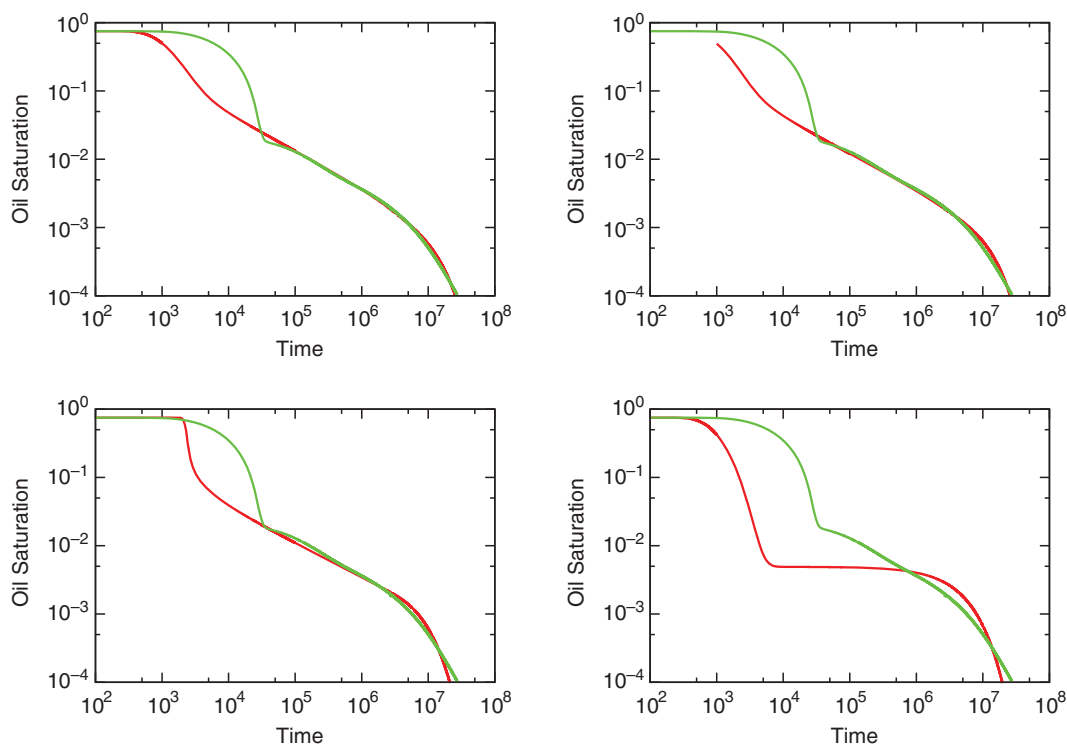


**Fig. 10—Breakthrough curves of the simulated oil saturation (green) at the producer at the right-side model boundary ( $x = 9$  m) for the Bristol Channel model (Fig. 7a) at a high flow rate of  $q = 10^{-4} \text{ m}^3 \cdot \text{m}^{-2} \cdot \text{s}^{-1}$  compared with the equivalent mass-transfer model (red): (Upper left) 3D diffusion in spherical inclusions for  $\tau_c = 9 \times 10^7$  seconds, (upper right) 2D diffusion into disks for  $\tau_c = 5 \times 10^7$  seconds, (lower left) 1D diffusion into slabs for  $\tau_c = 1.5 \times 10^7$  seconds, and (lower right) single-rate first-order mass transfer with  $\alpha = 2 \times 10^{-7} \cdot \text{s}^{-1}$ . Fracture porosity is  $\phi_f = 1.0 \times 10^{-2}$ , matrix porosity is  $\phi_m = 2.5 \times 10^{-1}$ , and the capillary diffusion coefficient in the fracture is set to  $D_f = 5 \times 10^{-4} \text{ m}^2 \cdot \text{s}^{-1}$ . Timescale is in seconds, as in Fig. 9.**

obtained with an MRMT model with a memory function that approximates the geometry of the matrix blocks as spheres with appropriate adjustment of the characteristic diffusion time  $\tau_c$  (see previous details). The classical first-order single-rate (i.e., standard dual-porosity) model underpredicts production after water breakthrough because it fails to capture the fast transfer rates comprised in the diffusion model (Fig. 10). We chose the rate  $\alpha$  such that the late-time tail is approximately matched. Similarly, excellent agreement between the simulated saturation breakthrough and equivalent MRMT models immediately can be achieved for the lower flow rates of  $q = 10^{-5} \text{ m}^3 \cdot \text{m}^{-2} \cdot \text{s}^{-1}$  (Fig. 11), for which the fracture dispersion coefficient  $D_f$  has been readjusted according to the lower flow rate, as outlined previously. The single-rate model still fails to capture the diffusion-controlled production behavior. The discrepancy between the simulated oil saturation and MRMT prediction after water breakthrough in the fractures is caused by the linearized flow model in the fractures, which cannot account for the rarefaction fan occurring during viscous-dominated flow in the mobile domain; this can be improved straightforwardly by selecting the full displacement model for the fracture, which is, however, not the focus of our work in which we are more interested in improving the prediction of the late-time production behavior.

## Summary and Outlook

We have introduced a novel MRMT model to simulate multiphase flow in fractured reservoirs and applied it successfully to improve the prediction of the late-time production behavior dominated by counter-current imbibition between fractures and matrix in a world-class outcrop analog of a fractured reservoir; in all cases, our MRMT model outperformed the classical first-order single-rate transfer model and provided a much improved prediction of the production behavior at late time for viscous-dominated flow. Our predictions were obtained by selecting the appropriate, and,

in part, easily determinable, macroscopic parameters (e.g., flow rates, fracture parameters) without extensive fitting procedures or computationally intensive history matching because computations are performed in the Laplace domain. Time-space solutions are obtained by numerical inverse Laplace transform.

Our model is similar to the first-order MRMT model for miscible single-phase flow developed by Haggerty and Gorelick (1995), which has been applied successfully to model the transport of a nonreactive tracer in fractured dolomite (Haggerty et al. 2001; McKenna et al. 2001). Similar to the classical single-rate dual-porosity model, the mass transfer of a fluid phase or dissolved chemical component between fracture and matrix is modeled by a source term. However, rather than allowing only for a single-transfer process described by a single transfer rate and shape factor, the structure of the matrix blocks and process parameters in the matrix are contained in a memory function, which is the kernel of the nonlocal source/sink term in the proposed two-phase MRMT model. This allows for more realistic modeling of transfer processes between fracture and matrix (e.g., the oil saturation in the matrix can increase or decrease) and does not approximate transfer between the fracture and matrix as a first-order process. Diffusion in the matrix blocks and therefore incomplete mixing (i.e., heterogeneous oil saturations) within the matrix are explicitly accounted for. As we saw, this has a significant impact on the prediction of the late-time breakthrough behavior.

The parameters describing the memory function have a clear physical meaning and can, in principle, be derived if the geometry and parameters of the substructure are known in detail (Gouze et al. 2008a,b). This means that, in turn, information about substructure can be inferred from the parameters describing the memory function, which has practical implications for reservoir simulation in dual-porosity systems. We thus see our model as a complement to existing fractured-reservoir modeling and simulation workflows. Many recent developments allow reservoir engineers to overcome well-known limitations in the classical dual-



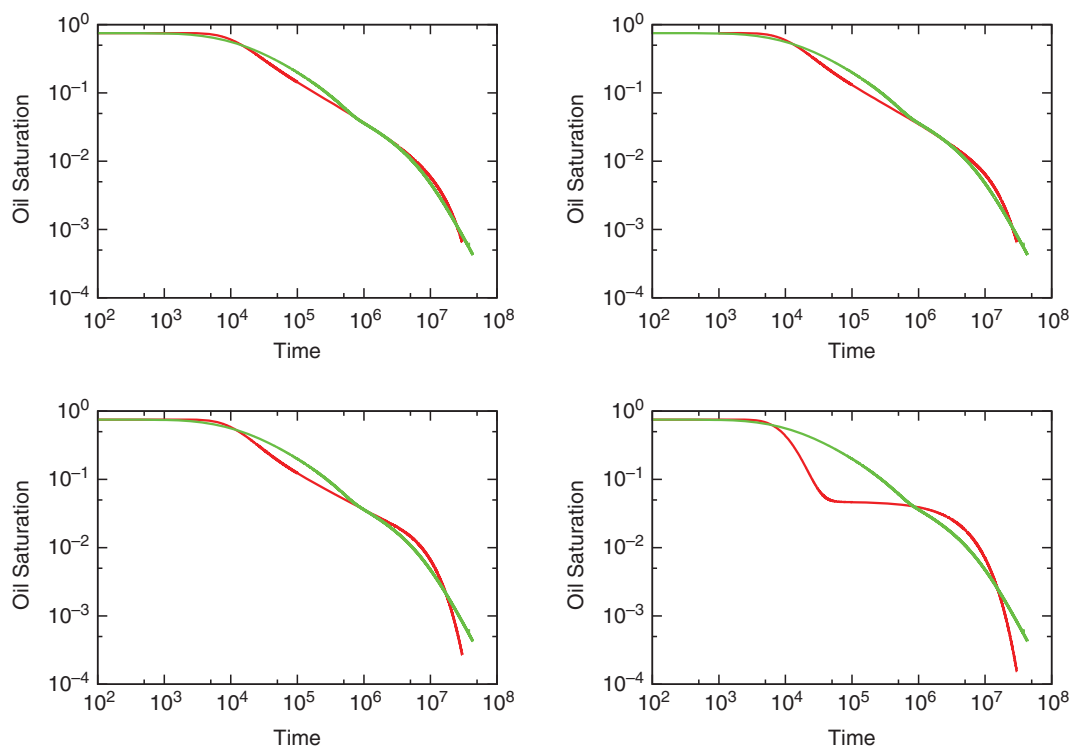


**Fig. 11**—The same as in Fig. 10 but for a low flow rate of  $q_w = 10^{-5} \text{ m}^3 \cdot \text{m}^{-2} \cdot \text{s}^{-1}$  and corresponding lower fracture dispersion coefficient of  $D_f = 5 \times 10^{-5} \text{ m}^2 \cdot \text{s}^{-1}$ .

porosity model. These include, but are not limited to, the following extensions: The multi-rate dual-porosity model of Di Donato et al. (2007) uses a distribution of first-order transfer functions to model the different transfer rates from distributions of matrix blocks with multiple sizes. The multiple interacting continua extension of the classical dual-porosity model (Pruess and Narasimhan, 1985; Karimi-Fard et al. 2006; Rubin 2007; Gong et al. 2008; Tatomir et al. 2011) allows for local variations in saturation or concentration in the matrix. Time-dependent shape factors can model unsteady-state processes such as partially immersed fractures and nonuniform matrix saturations (Rangel-German and Kovscek 2006; Rangel-German et al. 2010). These approaches are the numerical equivalent to our MRMT model: they attempt to approximate nonuniform saturation transients in the matrix and thus spatially and temporally varying transfer rates. Use of the presented MRMT model in a reservoir simulator is also possible, but it requires the implementation of a time convolution over the memory function. This (in principle) time-consuming operation may be implemented in an efficient way with the algorithm presented in Silva et al. (2009).

The drawbacks of these improved dual-porosity models are higher computational costs, and parameterizing and calibrating the associated parameters, typically using history matching, remains a challenge. This is in addition to common uncertainties encountered in history matching fractured reservoirs. We thus suggest that one could use the information contained in the memory function in our model to approximate key parameters and to investigate their related sensitivities as well as the impact of different dual-porosity-model extensions in theoretical studies on a well-by-well basis before beginning the full-field reservoir simulation. The estimation of the memory function could be aided by production data in fields with an extended production history, or (given the apparent similarities in the fracture-matrix exchange behavior during diffusion of nonreactive tracers and immiscible two-phase flow) by use of data from tracer tests in greenfields. In this instance, the memory function would need to be rescaled to account for the different magnitude of molecular diffusion of a tracer and capillary-driven diffusion during counter-current imbibition. Importantly, use of our MRMT model in traditional NFR

modeling and simulation workflows is computationally efficient because the estimation of the memory function in our model can be carried out in the Laplace domain if the fracture-flow model is linearized.

Future work on our MRMT model must include full 3D simulations with gravity-dominated flow processes because this is an important recovery mechanism in naturally fractured reservoirs (Al-Kobaisi et al. 2009; Ramirez et al. 2009). Thus, this is subject to our ongoing research. Whereas we believe that a formal mathematical derivation by use of homogenization for the inclusion of gravitational processes in the MRMT model for entire fracture networks is not possible, one should be able to perform this derivation for individual fracture-matrix systems. Buoyant flow in the matrix domain is analogous to advective transport in the matrix domain. Slow advective transport in the immobile domain can be modeled by a memory function as well (Lichtner and Kang 2007), and, in principle, these results can be transferred to two-phase-flow modeling to incorporate gravity effects. However, the reinfiltration of a buoyancy-driven fluid front through a matrix block into the matrix domain has to be considered. Incorporating slow advection in the memory function will serve us as the starting point to include gravitational processes on the basis of phenomenological rules.

## Nomenclature

- $a$  = dispersion length
- $c$  = concentration in immobile domain
- $C$  = solute concentration
- $D$  = capillary diffusion,  $\text{m}^2 \cdot \text{s}^{-1}$
- $D_{1p}$  = solute diffusion,  $\text{m}^2 \cdot \text{s}^{-1}$
- $f$  = fractional flow
- $g$  = acceleration caused by gravity,  $\text{m} \cdot \text{s}^{-2}$
- $g(r, t)$  = Green function
- $I$  = Bessel function
- $k$  = permeability,  $\text{m}^2$
- $k_r$  = relative permeability
- $l$  = characteristic length scale,  $\text{m}$
- $L$  = domain length,  $\text{m}$

$p$  = fluid pressure, Pa  
 $P_c$  = capillary pressure, Pa  
 $P_d$  = capillary entry pressure, Pa  
 $q$  = source/sink term,  $s^{-1}$   
 $r$  = 3D position vector in matrix block, m  
 $s$  = saturation in immobile domain  
 $S$  = saturation  
 $\hat{S}$  = endpoint saturation  
 $t$  = time, seconds  
 $T$  = transfer function,  $s^{-1}$   
 $v$  = Darcy velocity,  $m \cdot s^{-1}$   
 $V$  = volume,  $m^3$   
 $x$  = spatial coordinate, m  
 $z$  = depth, m  
 $x$  = 3D coordinate vector, m  
 $\alpha$  = transfer rate,  $s^{-1}$   
 $\beta$  = rate coefficient,  $s^{-1}$   
 $\gamma$  = fracture-matrix interface,  $m^2$   
 $\varepsilon$  = Corey exponent  
 $\Theta$  = Heaviside function  
 $\lambda$  = mobility,  $Pa^{-1} \cdot s^{-1}$   
 $\lambda$  = Laplace variable  
 $\mu$  = viscosity, Pa·s  
 $\mu(t)$  = memory function for two-phase flow  
 $\xi$  = integration variable  
 $\pi$  = frequency of immobile (matrix) domains  
 $\rho$  = fluid density,  $kg \cdot m^{-3}$   
 $\tau$  = characteristic timescale, seconds  
 $\phi$  = porosity  
 $\varphi(t)$  = memory function single-phase flow  
 $\chi$  = volume fraction of immobile (matrix) domain  
 $\Omega$  = matrix domain

## Subscripts

$c$  = capillary (imbibition)  
 $d$  = diffusion (solutes)  
 $eff$  = volume averaged property  
 $f$  = fracture (mobile) domain  
 $ir$  = irreducible  
 $I, ith$  = immobile domain  
 $m$  = matrix (immobile) domain  
 $n$  = counter  
 $o$  = oil  
 $r$  = coordinate in immobile domain  
 $w$  = water

## Superscript

\* = Laplace space

## Acknowledgments

We thank Karen Schmid for useful comments on the manuscript and the UK Engineering and Physical Sciences Research Council as well as Foundation CMG for financial support. Constructive comments by three reviewers have improved the quality of this manuscript.

## References

- Abramowitz, M. and Stegun, I.A. 1972. *Handbook of Mathematical Functions*. New York: Dover Publications.
- Abushaikh, A.S.A. and Gosselin, O. 2008. Matrix-Fracture Transfer Function in Dual-Medium Flow Simulation: Review, Comparison, and Validation. Paper SPE 113890 presented at the Europec/EAGE Conference and Exhibition, Rome, Italy, 9–12 June. <http://dx.doi.org/10.2118/113890-MS>.
- Al-Kobaisi, M., Kazemi, H., Ramirez, B. et al. 2009. A Critical Review for Proper use of Water/Oil/Gas Transfer Functions in Dual-Porosity Naturally Fractured Reservoirs: Part II. *SPE Res Eval & Eng* **12** (2): 211–217. <http://dx.doi.org/10.2118/124213-PA>.
- Babadagli, T., Hatiboglu, C.U., and Hamida, T. 2009. Evaluation of Matrix-Fracture Transfer Functions for Counter-current Capillary Imbibition. *Transp. Porous Med.* **80** (1): 17–56. <http://dx.doi.org/10.1007/s11242-009-9337-x>.
- Balogun, A., Kazemi, H., Ozkan, E. et al. 2009. Verification and Proper Use of Water-Oil Transfer Function for Dual-Porosity and Dual-Permeability Reservoirs. *SPE Res Eval & Eng* **12** (2): 189–199. <http://dx.doi.org/10.2118/104580-PA>.
- Bear, J. 1972. *Dynamics of Fluids in Porous Media*. Mineola, New York: Courier Dover Publications.
- Behbahani, H. and Blunt, M.J. 2005. Analysis of Imbibition in Mixed-Wet Rocks Using Pore-Scale Modeling. *SPE J.* **10** (4): 466–474. <http://dx.doi.org/10.2118/90132-PA>.
- Belayneh, M. 2004. Paleostress Orientation Inferred from Surface Morphology of Joints on the Southern Margin of the Bristol Channel Basin, UK. In *The Initiation, Propagation, and Arrest of Joints and Other Fractures*, ed. J.W. Cosgrove and T. Engelder, Vol. 231, pp. 243–255. London, England: Geological Society of London Special Publications.
- Belayneh, M., Geiger, S., and Matthäi, S.K. 2006. Numerical Simulation of Water Injection into Layered Fractured Carbonate Reservoir Analogs. *AAPG Bull.* **90** (10): 1473–1493. <http://dx.doi.org/10.1306/05090605153>.
- Belayneh, M.W., Matthäi, S.K., Blunt, M.J. et al. 2009. Comparison of Deterministic with Stochastic Fracture Models in Water-Flooding Numerical Simulations. *AAPG Bull.* **93** (11): 1633–1648. <http://dx.doi.org/10.1306/07220909031>.
- Bourbiaux, B., Basquet, R., Cacas, M.C. et al. 2002. An Integrated Workflow To Account for Multi-Scale Fractures in Reservoir Simulation Models: Implementation and Benefits. Paper SPE 78489 presented at the Abu Dhabi International Petroleum Exhibition and Conference, Abu Dhabi, UAE, 13–16 October. <http://dx.doi.org/10.2118/78489-MS>.
- Carrera, J., Sanchez-Vila, X., Benet, I. et al. 1998. On Matrix Diffusion: Formulations, Solution Methods and Qualitative Effects. *Hydrogeol. J.* **6** (1): 178–190. <http://dx.doi.org/10.1007/s100400050143>.
- Chen, Z., Huan, G., and Ma, Y. 2006. *Computational Methods for Multiphase Flows in Porous Media*, Vol. 2, Computational Science and Engineering Series. Manama, Bahrain: SIAM Publishers.
- Dershowitz, B., LaPointe, P., Eiben, T. et al. 2000. Integration of Discrete Feature Network Methods with Conventional Simulator Approaches. *SPE Res Eval & Eng* **3** (2): 165–170. <http://dx.doi.org/10.2118/62498-PA>.
- Di Donato, G., Lu, H.Y., Tavassoli, Z. et al. 2007. Multi-rate-Transfer Dual-Porosity Modeling of Gravity Drainage and Imbibition. *SPE J.* **12** (1): 77–88. <http://dx.doi.org/10.2118/93144-PA>.
- Eaton, J.W., Bateman, D., and Hauberg, S. 2011. *GNU Octave Version 3.0.1 Manual: A High-Level Interactive Language for Numerical Computations, Edition 3 for Octave version 3.6.1*. Tualatin/Portland, Oregon: CreateSpace Independent Publishing Platform.
- Garcia, M., Gouth, F., and Gosselin, O. 2007. Fast and Efficient Modeling and Conditioning of Naturally Fractured Reservoir Models Using Static and Dynamic Data. Paper SPE 107525 presented at the SPE Europec/EAGE Conference and Exhibition, London, United Kingdom, 11–14 June. <http://dx.doi.org/10.2118/107525-MS>.
- Geiger, S., Cortis, A., and Birkhölzer, J.T. 2010. Upscaling Solute Transport in Naturally Fractured Porous Media with the Continuous Time Random Walk Method. *Water Resour. Res.* **46**: W12530. <http://dx.doi.org/10.1029/2010WR009133>.
- Geiger, S. and Emmanuel, S. 2010. Non-Fourier Thermal Transport in Fractured Geological Media. *Water Resour. Res.* **46**: W07504. <http://dx.doi.org/10.1029/2009WR008671>.
- Geiger, S., Matthäi, S., Niessner, J. et al. 2009. Black-Oil Simulations for Three-Component, Three-Phase Flow in Fractured Porous Media. *SPE J.* **14** (2): 338–354. <http://dx.doi.org/10.2118/107485-PA>.
- Geiger, S., Roberts, S., Matthäi, S.K. et al. 2004. Combining Finite Element and Finite Volume Methods for Efficient Multiphase Flow Simulations in Highly Heterogeneous and Structurally Complex Geologic Media. *Geofluids* **4** (4): 284–299. <http://dx.doi.org/10.1111/j.1468-8123.2004.00093.x>.
- Gilman, J.R. and Kazemi, H. 1983. Improvements in Simulation of Naturally Fractured Reservoirs. *SPE J.* **23** (4): 695–707. <http://dx.doi.org/10.2118/10511-PA>.

- Gilman, J.R. and Kazemi, H. 1988. Improved Calculations for Viscous and Gravity Displacement in Matrix Blocks in Dual-Porosity Simulators. *J. Pet. Tech.* **40** (1): 60–70. <http://dx.doi.org/10.2118/16010-PA>.
- Gong, B., Karimi-Fard, M., and Durlafsky, L.J. 2008. Upscaling Discrete Fracture Characterizations to Dual-Porosity, Dual-Permeability Models for Efficient Simulation of Flow with Strong Gravitational Effects. *SPE J.* **13** (1): 58–67. <http://dx.doi.org/10.2118/102491-PA>.
- Gouze, P., Le Borgne, T., Leprovost, R. et al. 2008a. Non-Fickian Dispersion in Porous Media: 1. Multi-Scale Measurements Using Single Well Injection Withdrawal Tracer Tests at the Ses Sitjoles/Aliañce Test Site (Spain). *Water Resour. Res.* **44**: W06426. <http://dx.doi.org/10.1029/2007WR006278>.
- Gouze, P., Melean, Y., Le Borgne, T. et al. 2008b. Non-Fickian Dispersion in Porous Media Explained by Heterogeneous Microscale Matrix Diffusion. *Water Resour. Res.* **44**: W11416. <http://dx.doi.org/10.1029/2007WR006690>.
- Haggerty, R., Fleming, S.W., Meigs, L.C. et al. 2001. Tracer Tests in a Fractured Dolomite: 2. Analysis of Mass Transfer in Single-Well Injection-Withdrawal Tests. *Water Resour. Res.* **37** (5): 1129–1142. <http://dx.doi.org/10.1029/2000WR900334>.
- Haggerty, R. and Gorelick, S.M. 1995. Multiple-Rate Mass Transfer for Modelling Diffusion and Surface Reactions in Media with Pore-Scale Heterogeneity. *Water Resour. Res.* **31** (10): 2383–2400. <http://dx.doi.org/10.1029/95WR10583>.
- Harvey, C.F. and Gorelick S.M. 1995. Temporal Moment-Generating Equations: Modeling Transport and Mass Transfer in Heterogeneous Aquifers. *Water Resour. Res.* **31** (8): 1895–1911. <http://dx.doi.org/10.1029/95WR01231>.
- Hassanzadeh, H. and Pooladi-Darvish, M. 2006. Effects of Fracture Boundary Conditions on Matrix-Fracture Transfer Shape Factor. *Transp. Porous Med.* **64** (1): 51–71. <http://dx.doi.org/10.1007/s11242-005-1398-x>.
- Hoteit, H. and Firoozabadi, A. 2008. Numerical Modeling of Two-Phase Flow in Heterogeneous Permeable Media with Different Capillarity Pressures. *Adv. Water Resour.* **31** (1): 56–73. <http://dx.doi.org/10.1016/j.advwatres.2007.06.006>.
- Karimi-Fard, M., Gong, B., and Durlafsky, L.J. 2006. Generation of Coarse-Scale Continuum Flow Models from Detailed Fracture Characterizations. *Water Resour. Res.* **42** (10): W10423. <http://dx.doi.org/10.1029/2006WR005015>.
- Kazemi, H. and Gilman, J.R. 1993. Multiphase Flow in Fractured Petroleum Reservoirs. In *Flow and Contaminant Transport in Fractured Rock*, ed. J. Bear, C.-F. Tsang, and G. de Marsily, pp. 267–323. San Diego, California: Academic Press Inc.
- Kazemi, H., Merrill, L.S., Porterfield, K.L. et al. 1976. Numerical Simulation of Water-Oil Flow in Naturally Fractured Reservoirs. *SPE J.* **16** (6): 317–326. <http://dx.doi.org/10.2118/5719-PA>.
- Lichtner, P.C. and Kang, Q. 2007. Upscaling Pore-Scale Reactive Transport Equations Using a Multiscale Continuum Formulation. *Water Resour. Res.* **43** (12): W12S15. <http://dx.doi.org/10.1029/2006WR005664>.
- Lim, K.T. and Aziz, K. 1995. Matrix-Fracture Transfer Shape Factors for Dual-Porosity Simulators. *J. Pet. Sci. Eng.* **13** (3): 169–178. [http://dx.doi.org/10.1016/0920-4105\(95\)00010-F](http://dx.doi.org/10.1016/0920-4105(95)00010-F).
- Lu, H.Y., Di Donato, G., and Blunt, M.J. 2008. General Transfer Functions for Multiphase Flow in Fractured Reservoirs. *SPE J.* **13** (3): 289–297. <http://dx.doi.org/10.2118/102542-PA>.
- Ma, S., Morrow, N.R., and Zhang, X. 1997. Generalized Scaling of Spontaneous Imbibition Data for Strongly Water-Wet Systems. *J. Pet. Sci. Eng.* **18** (3): 165–178. [http://dx.doi.org/10.1016/S0920-4105\(97\)00020-X](http://dx.doi.org/10.1016/S0920-4105(97)00020-X).
- Mason, G., Fischer, H., Morrow, N.R. et al. 2010. Correlation for the Effect of Fluid Viscosities on Counter-current Spontaneous Imbibition. *J. Pet. Sci. Eng.* **72** (1): 195–205. <http://dx.doi.org/10.1016/j.petrol.2010.03.017>.
- Matthäi, S.K. and Belayneh, M. 2004. Fluid Flow Partitioning Between Fractures and a Permeable Rock Matrix. *Geophys. Res. Lett.* **31** (7): L07602. <http://dx.doi.org/10.1029/2003GL019027>.
- Matthäi, S.K., Geiger, S., Roberts, S.G. et al. 2007. Numerical Simulations of Multiphase Fluid Flow in Structurally Complex Reservoirs. In *Structurally Complex Reservoirs*, ed. S.J. Jolley, D. Barr, J.J. Walsh, and R.J. Knipe, Vol. 292, pp. 405–429. London, England: Geological Society of London Special Publications. <http://dx.doi.org/10.1144/SP292.22>.
- McKenna, S.A., Meigs, L.C., and Haggerty, R. 2001. Tracer Tests in a Fractured Dolomite, 3. Double-Porosity, Multi-Rate Mass Transfer Processes in Convergent Flow Tracer Tests. *Water Resour. Res.* **37** (5): 1143–1154. <http://dx.doi.org/10.1029/2000WR900333>.
- Pruess, K. and Narasimhan, T.N. 1985. A Practical Method for Modeling Fluid and Heat Flow in Fractured Porous Media. *SPE J.* **25** (1): 14–26. <http://dx.doi.org/10.2118/10509-PA>.
- Quandalle, P. and Sabathier, J.C. 1989. Typical Features of a Multipurpose Reservoir Simulator *SPE Res Eng* **4** (4): 475–480. <http://dx.doi.org/10.2118/16007-PA>.
- Ramirez, B., Kazemi, H., Al-Kobaisi, M. et al. 2009. A Critical Review for Proper Use of Water/Oil/Gas Transfer Functions in Dual-Porosity Naturally Fractured Reservoirs: Part I. *SPE Res Eval & Eng* **12** (2): 200–217. <http://dx.doi.org/10.2118/124213-PA>.
- Rangel-German, E.R. and Kovscek, A.R. 2006. Time-Dependent Matrix-Fracture Shape Factors for Partially and Completely Immersed Fractures. *J. Pet. Sci. Eng. Geol.* **54** (3–4): 149–163. <http://dx.doi.org/10.1016/j.petrol.2006.08.004>.
- Rangel-German, E.R., Kovscek, A.R., and Akin, S. 2010. Time-Dependent Shape Factors for Uniform and Non-Uniform Pressure Boundary Conditions. *Transp. Porous Med.* **83** (3): 591–601. <http://dx.doi.org/10.1007/s11242-009-9461-7>.
- Reichenberger, V., Jakobs, H., Bastian, P. et al. 2006. A Mixed-Dimensional Finite Volume Method for Two-Phase Flow in Fractured Porous Media. *Adv. Water Resour.* **29** (7): 1020–1036. <http://dx.doi.org/10.1016/j.advwatres.2005.09.001>.
- Rubin, B. 2007. Simulating Gravity Drainage and Reinfiltration with a Subdomain-Dual-Permeability Hybrid Fracture Model. Paper SPE 106191 presented at the SPE Reservoir Simulation Symposium, Houston, Texas, 26–28 February. <http://dx.doi.org/10.2118/106191-MS>.
- Schmid, K.S. and Geiger, S. 2012. Universal Scaling of Spontaneous Imbibition for Water-Wet Systems. *Water Resour. Res.* **48**: W03507. <http://dx.doi.org/10.1029/2011WR011566>.
- Silva, O., Carrera, J., Kumar, S. et al. 2009. A General Real-Time Formulation for Multi-Rate Mass Transfer Problems. *Hydrol. Earth Syst. Sci.* **6** (2): 2415–2449. <http://dx.doi.org/10.5194/hessd-6-2415-2009>.
- Tatomir, A.B., Szymkiewicz, A., Class, H. et al. 2011. Modeling Two-Phase Flow in Large Scale Fractured Porous Media with an Extended Multiple Interacting Continua Method. *CMES: Computer Modelling in Eng. Sci.* **77** (2): 81–112. <http://dx.doi.org/10.3970/cmcs.2011.077.081>.
- Tavassoli, Z., Zimmerman, R.W., and Blunt, M.J. 2005. Analytic Analysis for Oil Recovery During Counter-current Imbibition in Strongly Water-Wet Systems. *Transp. Porous Med.* **58**: 173–189. <http://dx.doi.org/10.1007/s11242-004-5474-4>.
- Warren, J.E. and Root, P.J. 1963. The Behavior of Naturally Fractured Reservoirs. *SPE J.* **3** (3): 245–255. <http://dx.doi.org/10.2118/426-PA>.
- Zimmerman, R.W., Chen, G., Hadgu, T. et al. 1993. A Numerical Dual-Porosity Model with Semianalytical Treatment of Fracture/Matrix Flow. *Water Resour. Res.* **29** (7): 2127–2137. <http://dx.doi.org/10.1029/93WR00749>.

**Sebastian Geiger** is the Foundation CMG Chair for Carbonate Reservoir Simulation at the Institute of Petroleum Engineering, Heriot-Watt University, in which he leads the carbonate research group. Geiger is also the codirector of the International Centre for Carbonate Reservoirs in Edinburgh, a joint research alliance between Heriot-Watt University and University of Edinburgh. His current research interests include modeling, simulating, and upscaling multiphase-flow processes in (fractured) carbonate reservoirs, enhanced-oil-recovery processes for carbonate reservoirs, and studying the fundamental transport processes in carbonates from a pore-scale perspective. Geiger holds a PhD degree from Eidgenössische Technische Hochschule Zürich in 2004 and worked at ETH Zurich as a post-doctoral researcher. He holds an MSc degree from Oregon State University and a Vordiplom from the University of Freiburg, Germany. Geiger joined Heriot-Watt University in 2006 as a lecturer and became a full professor in 2010. He is a member of SPE, European Association of Geoscientists and Engineers (EAGE), the American Association of Petroleum Geologists, the American Geophysical Union (AGU), and




Interpore and has served on numerous SPE and EAGE technical committees.

**Marco Dentz** is professor at the Institute of Environmental Assessment and Water Research (IDAEA) of the Spanish National Research Council (CSIC) in Barcelona, Spain. His research focuses on the understanding of flow, transport, and reaction processes across scales in heterogeneous media. Dentz holds a Diploma degree in physics from Ruperto-Carola University in Heidelberg, Germany, at which he also earned a PhD degree. After that Dentz was a Minerva Fellow at the Department of Environmental Sciences and Energy Research at the Weizmann Institute of Science, Israel. At the end of 2002, he joined the Technical University of Catalonia, in Barcelona, where he received a Ramon y Cajal Fellowship of the Spanish Ministry of Science and Technology. In May 2009, Dentz moved to the IDAEA-CSIC in which he was offered the

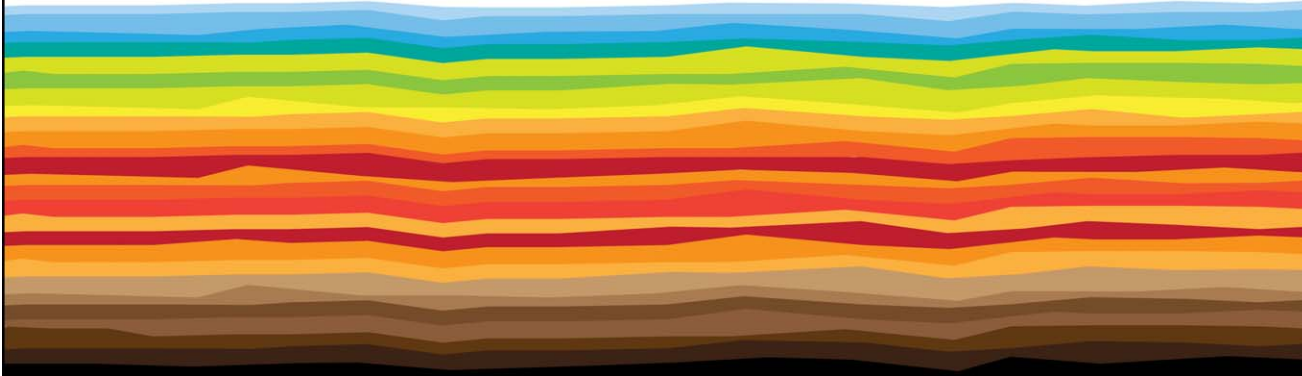
position of a Profesor de Investigación. He is a member of the AGU and the German Physical Society.

**Insa Neuweiler** has been a full professor of fluid mechanics and environmental physics in civil engineering at the Leibniz Universität, Hannover, Germany, since 2008. Her research interests are the upscaling of flow and transport problems, stochastic modeling, two-phase-flow processes, modeling of vadose-zone flow processes, and data assimilation for subsurface flow problems. Neuweiler holds a diploma degree in physics from the University of Heidelberg and a doctoral degree in environmental sciences from ETH Zurich. She worked as a post-doctoral researcher at Imperial College London and was leader of an Emmy Noether research group at the University of Stuttgart, funded by the German Science Foundation. Neuweiler is a member of AGU, Society of Industrial and Applied Mathematics, and Interpore.



## SPE Web Events


EXPERTS • TECHNOLOGY • EDUCATION



### Dig deeper without leaving your desk.


Too busy to be away from the office? Take yourself to greater depths right from your desktop with SPE Web Events. Join our industry experts as they explore solutions to real problems and discuss trending topics.

View a list of available web events at [www.spe.org/events/webevents](http://www.spe.org/events/webevents).



Society of Petroleum Engineers

Connect, share with us on



@SPE\_Events  
#SPEWEBEVENTS